A parabolic linear evolution equation for cellular detonation instability

By Mark Short

Theoretical and Applied Mechanics, University of Illinois, Urbana, IL 61801.

Using the combined limits of a large activation energy and a ratio of specific heats close to unity, a dispersion relation has recently been derived which governs the stability of a steady Chapman-Jouguet detonation wave to two-dimensional linear disturbances. The analysis considers instability evolution time-scales that are long on the time-scale of fluid particle passage through the main reaction layer. In the following, a simplified polynomial form of the dispersion relation is derived under an appropriate choice of a distinguished limit between an instability evolution time-scale that is long on the time-scale of particle passage through the induction zone and a transverse disturbance wavelength that is long compared to the hydrodynamic thickness of the induction zone. A third-order in time, sixth-order in space, parabolic linear evolution equation is derived which governs the initial dynamics of cellular detonation formation. The linear dispersion relation is shown to have the properties of a most unstable wavenumber, leading to a theoretical prediction of the initial detonation cell-spacing, and a wavenumber above which all disturbances decay, eliminating the growth of small-wavelength perturbations. The role played by curvature of the detonation front in the dynamics of the cellular instability is also highlighted.

1. Introduction

Using combined limits of near Chapman-Jouguet detonation velocity, large dimensionless activation energy, long-wavelength shock perturbations on the scale of the induction zone thickness and slow dynamic shock evolution measured on the time scale of particle passage through the induction zone, Yao and Stewart (1996) have recently derived a two-dimensional hyperbolic nonlinear evolution equation for the motion of an unstable detonation wave. This evolution equation is a partial differential equation in the shock displacement, and is a relation associating the normal shock velocity, the first and second time derivatives of the normal shock velocity, the shock curvature, and the first normal time derivative of the shock curvature. The equation is third-order in time and second-order in space. The domain of detonation parameters in which the nonlinear equation will predict cellular patterns has been analysed in Stewart, Aslam and Yao (1996), and has been determined as the unstable regimes in which the two wave operators present in the linearised version of the evolution equation are hyperbolic. The higher-order hyperbolic wave operator connects the second time derivative of the normal shock velocity to the first time derivative of the detonation front curvature and has an associated wave speed a. The second wave operator connects the first

derivative of the normal shock velocity to the curvature of the detonation front, and in regions where it is sub-hyperbolic, i.e. for parameter regimes which predict the decay of one-dimensional linear disturbances, it has an associated wave speed a_{sub}. Detonation cells are thus predicted in regimes where $a_{sub}^2 > a^2$.

Despite the clear success of the Stewart-Yao equation in modelling the dynamics of cellular detonation patterns, there are two particular features of the numerically evaluated linear dispersion spectra (Short 1997) that are not present in the linearised Stewart-Yao equation. Firstly, the dispersion relation does not possess a local maximum growth rate in finite transverse wavenumber space and so cannot predict the cell-wavelengths which are initially the most unstable. Secondly, it does not possess a critical wavenumber above which all linear disturbances decay. This corresponds to an important feature of detonation wave propagation whereby cell formation does not occur in very narrow channels, and implies that small wavelength disturbances are prevented from amplifying. The lack of these two properties indicates a need for a more general linear theory to be developed.

The required generalisation of the linear dispersion relation is also reflected in the studies by Buckmaster & Ludford (1986) and Buckmaster (1989). Buckmaster & Ludford (1986) consider long-wavelength perturbations of the order of the activation energy times the induction zone length and an instability evolution time-scale of the order of the activation energy times the particle transit time through the induction zone. Under this distinguished limit, they found a single unstable but real mode, whose growth rate increased monotonically with wavenumber and so does not lead to a prediction of a characteristic initial cell-spacing. Subsequently, Buckmaster (1989) conducted an analysis in which the disturbance wavelength scaling is taken to be of the order of the square root of the activation energy times the induction zone length. This scaling introduces an important modification, which is that the curvature of the front now plays a crucial role in determining the induction zone structure. Buckmaster (1989) again found a single unstable real mode, but this now featured an explicit maximum growth rate at a finite wavenumber, as well as a wavenumber above which the linear disturbance decayed. Buckmaster (1989) proposed that the former property could be associated with the possible prediction of a unique initial detonation cell-spacing. Being real, however, the unstable mode does not propagate transverse to the front, but nevertheless, a possible physical mechanism for cell formation does arise in such cases (Buckmaster 1988). Short (1997) has found that the asymptotic results of Buckmaster and Ludford (1986) and Buckmaster (1989) can only be recovered numerically in the limit of very large activation energies.

Using a different asymptotic strategy, Short and Stewart (1997) have recently derived an analytical dispersion relation for two-dimensional Chapman-Jouguet linear detonation instability, under the two assumptions of a large activation energy in the steady detonation wave structure and a ratio of specific heats close to unity. The latter limit was first introduced in the context of an analytical solution of the Clarke equation (1981) in a shock-induced ignition problem by Blythe and Crighton (1989), and was subsequently used by Short (1996) to derive an analytical dispersion relation for the classical limiting square-wave detonation model. The dispersion relation derived in Short and Stewart (1997) is valid for instability evolution time-scales that are long on the time-scale of particle passage through the main reaction layer and for transverse disturbance wavelengths that are long compared to the hydrodynamic thickness of the main reaction layer.

The main reaction layer can then be treated as a Rankine-Hugoniot discontinuity with heat addition. Thus for sufficiently large activation energies, the range of disturbance frequencies described by the analysis can be much higher than the inverse time-scale of particle passage through the induction zone, whereas the range of wavelengths can be much smaller than the hydrodynamic thickness of the induction zone. The analytical dispersion relation derived in Short and Stewart (1997) is shown to possess all the desirable characteristics of the behaviour of actual linear instability spectra. These include the predictions of critical finite wavenumbers at which maximum modal growth rates are attained, as well as critical finite wavenumbers above which disturbances decay. The main drawback with the analysis in Short & Stewart (1997) is that the dispersion relation is a highly complex, exponential function of the growth rate, frequency and wavelength of the disturbance.

As stated in Short and Stewart (1997), however, simplified polynomial versions of the dispersion relation are possible and these are pursued in the following article. This simplification occurs in situations where the disturbance frequency is low on the inverse time-scale of particle passage through the induction zone, and when the characteristic transverse disturbance wavelength is long compared to the hydrodynamic thickness of the induction zone. In these circumstances, the low-frequency, long-wavelength results of Buckmaster and Ludford (1986), Buckmaster (1989), as specialized to a Chapman-Jouguet detonation, and Yao & Stewart (1996) can then be recovered.

The present study analyses the properties of two linear evolution equations corresponding to simplified polynomial dispersion relations derived by exploiting two distinguished limits between the disturbance frequency and wavenumber in a low-frequency, long-wavelength expansion of the dispersion relation obtained in Short and Stewart (1997). In both cases the corresponding one-dimensional evolution equation is third-order in time. In situations where the disturbance wavelength is of the order of the inverse frequency, a third-order in time, second-order in space evolution equation is derived with a form similar to that derived in Yao & Stewart (1996). This is shown to have the same deficiencies in its representation of the linear dispersion relation. In contrast, in situations where the square root of the disturbance wavelength is of the order of the inverse of the disturbance frequency, a parabolic evolution equation is derived which is third-order in time and sixth-order in space. For the large range of detonation parameters in which there is a single unstable oscillatory mode in the actual linear stability spectra, the dispersion relation corresponding to this parabolic evolution equation gives a good qualitative understanding of the dynamics associated with the two-dimensionally unstable mode. This includes the presence of a maximum growth rate at a finite wavelength and a wavenumber above which two-dimensional disturbances decay. Predictions of two-dimensional neutral stability curves are also given. It appears that the global generic features of the parabolic equation make it a favourable candidate for predicting the dynamics of the onset of cellular detonation.

Before proceeding, we note that detonation stability studies using the large activation energy, square-wave model have been criticised in the past for possessing the so-called 'Zaidel pathology', where the stability spectrum consists of an infinite number of unstable modes whose growth rates increase with increasing frequency. Zaidel's model (1961) is, however, ad-hoc, replacing the main reaction layer or fire by a discontinuity with no spatial structure. In contrast, a rational

analysis based on large activation energy asymptotics (Buckmaster & Neves 1988) reveals a non-uniformity in the high-frequency expansions when the disturbance frequency is of the order of the inverse particle transit time through the main reaction layer. The non-uniformity must be resolved for a correct asymptotic description, and numerical solutions (Short 1997) reveal that disturbances with a frequency much higher than the scales defined by the fire thickness are stable. In contrast the spectrum obtained by Zaidel, where the fire has no structure, predicts an infinite number of unstable modes. However, the trend towards an ever increasing number of unstable modes can be captured numerically as the activation energy is increased (Short 1997). That said, it should be emphasised that the behaviour of the spectrum at high frequencies has, of course, no bearing at all on our ability to accurately describe the nature of the low-frequency instability for finite activation energies based on a truncated asymptotic expansion that is valid in the limit of large activation energies. This is the approach taken by Buckmaster & Ludford (1986), Buckmaster (1989), Yao & Stewart (1996) and is the approach taken here. Moreover, the overwhelming evidence from both experimental and numerical studies on two-dimensional detonation wave propagation is that low-frequency, long-wavelength disturbances control the dynamics of detonation instability, precisely the regime in which the aforementioned asymptotic studies are concerned.

The layout of the paper is as follows. In §2 & §3 an alternative derivation of the linear dispersion relation obtained by Short & Stewart (1997) is given. This demonstrates the interesting result that the weakly nonlinear induction zone dynamics of an unstable detonation wave are controlled by a generalised mean-flow form of the Clarke equation (1981). In §4, a one-dimensional linear evolution equation is derived governing the initial dynamics of a pulsating detonation front. In §5 the two-dimensional hyperbolic linear evolution equation is derived, whereas in §6 the two-dimensional parabolic linear evolution equation is derived, and its generic properties investigated.

2. Nonlinear evolution analysis

The nonlinear problem representing the response of a steady planar detonation wave to two-dimensional shock disturbances with an amplitude of the order of the inverse activation energy is formulated by defining an unsteady shock-attached coordinate system

$$x = X - \frac{1}{\theta}\hat{h}(y,t), \quad \theta \gg 1, \tag{2.1}$$

where $\hat{h}(y,t)$ is the $O(\theta^{-1})$ shock displacement relative to the steady shock location $X = 0$, and θ is the activation energy for the one-step reaction. The plane $x = 0$ denotes the shock position in the new coordinate system. The hydrodynamic behaviour of a detonation in an ideal gas undergoing an irreversible, unimolecular reaction with an Arrenhius rate constant is modelled by the system

$$\mathbf{z}_{,t} + \mathbf{A}\cdot\mathbf{z}_{,x} + \mathbf{B}\cdot\mathbf{z}_{,y} - \frac{1}{\theta}\hat{h}_{,t}\mathbf{z}_{,x} - \frac{1}{\theta}\hat{h}_{,y}\mathbf{B}\cdot\mathbf{z}_{,x} = \mathbf{c}, \tag{2.2}$$

where

$$\mathbf{z} = [\rho,\ u,\ v,\ p,\ T,\ Y]^{\mathrm{T}}, \tag{2.3}$$

for non-dimensional density ρ, normal velocity u, transverse velocity v, pressure p, temperature T and fuel mass fraction Y. The dimensional scalings for temperature, density and velocity are the steady detonation post-shock temperature, density and sound speed respectively. In particular, the length-scale is the steady induction zone length in the limit of large activation energy, whereas the time-scale is the time taken for an acoustic disturbance to propagate across the induction zone. The chemical matrix $\mathbf{c}$ is defined as

$$\mathbf{c} = [0,\ 0,\ 0,\ -\beta\rho r,\ -\gamma\beta r,\ \ r]^{\mathrm{T}} \tag{2.4}$$

where the reaction rate r is given by

$$r = -\frac{\mathcal{K}}{\theta\beta} Y \exp\left[\theta\left(1 - \frac{1}{T}\right)\right], \tag{2.5}$$

and the constant $\mathcal{K}$ by

$$\mathcal{K} = \frac{M_s(M_s^2 - 1)}{(\gamma M_s^2 - 1)}, \tag{2.6}$$

where M_s is post-shock steady-flow Mach number. The constant γ is the ratio of specific heats, while the constant β is the non-dimensional heat release scaled with respect to the post-shock thermal energy. Finally the matrices $\mathbf{A}$ and $\mathbf{B}$ are defined as,

$$\mathbf{A} = \begin{bmatrix} u & \rho & 0 & 0 & 0 & 0 \\ 0 & u & 0 & 1/\rho & 0 & 0 \\ 0 & 0 & u & 0 & 0 & 0 \\ 0 & \gamma p & 0 & u & 0 & 0 \\ 0 & (\gamma-1)T & 0 & 0 & u & 0 \\ 0 & 0 & 0 & 0 & 0 & u \end{bmatrix}, \quad \mathbf{B} = \begin{bmatrix} v & 0 & \rho & 0 & 0 & 0 \\ 0 & v & 0 & 0 & 0 & 0 \\ 0 & 0 & v & 1/\rho & 0 & 0 \\ 0 & 0 & \gamma p & v & 0 & 0 \\ 0 & 0 & (\gamma-1)T & 0 & v & 0 \\ 0 & 0 & 0 & 0 & 0 & v \end{bmatrix}. \tag{2.7}$$

Short & Stewart (1997) describe a linear stability analysis concerned with infinitesimal perturbations of the shock front. Below we present an alternative derivation of these results which explores a weakly nonlinear formulation based on $O(\theta^{-1})$ perturbations of the shock front. We demonstrate how a two-dimensional, mean-flow generalised form of the Clarke equation (1981) controls the detonation dynamics in the induction zone. The linear stability results of Short and Stewart (1997) are easily recovered from the weakly nonlinear formulation.

(*a*) *Induction zone analysis*

The induction zone response to two-dimensional detonation shock perturbations with an amplitude of the order of the inverse activation energy θ^{-1}, $\theta \gg 1$, is determined through the expansion,

$$\mathbf{z} = \mathbf{z}_s^* + \frac{1}{\theta}\hat{\mathbf{z}}(x, y, t) + \cdots, \tag{2.8}$$

where

$$\mathbf{z}_s^* = [1,\ M_s,\ 0,\ 1/\gamma,\ 1,\ 1]^{\mathrm{T}} \tag{2.9}$$

is the underlying steady post-shock state. Correspondingly, the matrices $\mathbf{A}$, $\mathbf{B}$ and $\mathbf{c}$ can be shown to take the following asymptotic form in the induction zone,

$$\begin{gathered}\mathbf{A}(;\theta) = \mathbf{A}_0^* + \frac{1}{\theta}\mathbf{A}_1(\hat{\mathbf{z}}) + \cdots, \quad \mathbf{B}(;\theta) = \mathbf{B}_0^* + \frac{1}{\theta}\mathbf{B}_1(\hat{\mathbf{z}}) + \cdots, \\ \mathbf{c}(;\theta) = \frac{1}{\theta}\mathbf{c}_1^* e^{\widehat{T}},\end{gathered} \tag{2.10}$$

where

$$\mathbf{A}_0^* = \begin{bmatrix} M_s & 1 & 0 & 0 & 0 & 0 \\ 0 & M_s & 0 & 1 & 0 & 0 \\ 0 & 0 & M_s & 0 & 0 & 0 \\ 0 & 1 & 0 & M_s & 0 & 0 \\ 0 & (\gamma-1) & 0 & 0 & M_s & 0 \\ 0 & 0 & 0 & 0 & 0 & M_s \end{bmatrix}, \quad \mathbf{B}_0^* = \begin{bmatrix} 0 & 0 & 1 & 0 & 0 & 0 \\ 0 & 0 & 0 & 0 & 0 & 0 \\ 0 & 0 & 0 & 1 & 0 & 0 \\ 0 & 0 & 1 & 0 & 0 & 0 \\ 0 & 0 & (\gamma-1) & 0 & 0 & 0 \\ 0 & 0 & 0 & 0 & 0 & 0 \end{bmatrix}, \tag{2.11}$$

and

$$\mathbf{c}_1^* = \left[0,\ 0,\ 0, 1, \gamma, -\beta^{-1}\right]^{\mathrm{T}}. \tag{2.12}$$

Thus the matrices $\mathbf{A}$ and $\mathbf{B}$ are constant to leading order in the induction zone in an expansion in θ^{-1}, while $\mathbf{c}$ is proportional to the temperature perturbation $\widehat{T}$ at $O(\theta^{-1})$. The problem for $\hat{\mathbf{z}}$ is determined by the reduced matrix system

$$\hat{\mathbf{z}}_{,t} + \mathbf{A}_0^* \cdot \hat{\mathbf{z}}_{,x} + \mathbf{B}_0^* \cdot \hat{\mathbf{z}}_{,y} = \mathbf{c}_1^* e^{\widehat{T}}. \tag{2.13}$$

Elimination of $\hat{\rho}$, $\hat{u}$, $\hat{v}$ and $\hat{p}$ from (2.13) leads to an equation for $\widehat{T}$ in the form

$$\begin{gathered}\left[\partial_{,t} + M_s\partial_{,x}\right]\left(\left[\partial_{,t} + M_s\partial_{,x}\right]^2 \widehat{T} - \nabla^2\widehat{T}\right) \\ -\gamma\left(\left[\partial_{,t} + M_s\partial_{,x}\right]^2\left[e^{\widehat{T}}\right] - \frac{1}{\gamma}\nabla^2\left[e^{\widehat{T}}\right]\right) = 0,\end{gathered} \tag{2.14}$$

where

$$\nabla^2 = \partial_{,xx} + \partial_{,yy}. \tag{2.15}$$

The equation (2.14) represents a two-dimensional generalisation of the Clarke equation (Clarke 1981) in a mean flow, and has been derived by considering perturbations of the steady detonation shock which are explicitly $O(\theta^{-1})$. Thus it is apparent that a generalized version of the Clarke equation governs the induction zone dynamics of cellular detonation instability.

The shock conditions for the perturbation variables are determined from the perturbed Rankine-Hugoniot relations across the detonation shock and are given

by

$$\hat{\rho} = \kappa_\rho \hat{h}_t, \quad \hat{u} = \kappa_u \hat{h}_t, \quad \hat{v} = \kappa_v \hat{h}_y, \quad \hat{p} = \kappa_p \hat{h}_t, \quad \widehat{T} = (\gamma - 1)\kappa_T \hat{h}_t, \quad \widehat{Y} = 0, \tag{2.16}$$

where

$$\begin{aligned}
\kappa_\rho &= \frac{(\mu - 1)M_s}{\mu(M_s^2 - 1)}\left(2 - (\gamma - 1)[\mu - 1]\right), \\
\kappa_u &= \frac{(\mu - 1)}{\mu(M_s^2 - 1)}\left(-(1 + M_s^2) + (\gamma - 1)[\mu - 1]M_s^2\right), \\
\kappa_v &= (\mu - 1)M_s, \\
\kappa_p &= \frac{(\mu - 1)M_s}{\mu(M_s^2 - 1)}\left(2 - (\gamma - 1)[\mu - 1]M_s^2\right), \\
\kappa_T &= \frac{(\mu - 1)M_s}{\mu(M_s^2 - 1)}\left(2 + (\mu - 1)(1 - M_s^2) - (\gamma - 1)[\mu - 1]M_s^2\right),
\end{aligned} \tag{2.17}$$

with the conditions (2.16) applied at $x = 0$. For a given Chapman-Jouguet detonation velocity D_{CJ} relative to the ambient atmosphere, the parameter μ, which represents the density jump across the steady detonation shock, and M_s are given by

$$\mu = \frac{(\gamma + 1)D_{CJ}^2}{2 + (\gamma - 1)D_{CJ}^2}, \quad M_s^2 = \frac{2 + (\gamma - 1)D_{CJ}^2}{2\gamma D_{CJ}^2 - (\gamma - 1)}. \tag{2.18}$$

(*b*) *Burnt zone analysis*

For Chapman-Jouguet detonation velocities, the outflow from the rear of the main reaction layer is sonic. For general detonation velocities, the flow in the burnt region is determined in the unsteady form

$$\mathbf{z} = \mathbf{z}_b(x, y, t), \tag{2.19}$$

where, for large activation energies, the flow is considered chemically inert. The flow solution can easily be represented in terms of the standard characteristic surfaces σ_L, σ_R and σ_P, where σ_L represents upstream acoustic propagation from infinity to the rear of the main reaction zone, σ_R downstream acoustic propagation away from the rear of the main reaction layer, while σ_P represents the paths of entropy and vorticity propagation. The amplitude of unsteady flow in the burnt zone will be a function of the characteristic frequency and wavelength of the shock perturbation. For sonic outflow, a condition on the equilibrium flow arises that eliminates the upstream characteristic path σ_L at the rear of the main reaction layer. Along this surface the burnt flow condition will then take the form of a compatibility condition depending on σ_R and σ_P having the form,

$$\mathbf{z}_b(\sigma_R, \sigma_P) = 0. \tag{2.20}$$

(*c*) *Matching*

When the disturbance frequency is low on the inverse time-scale of particle passage through the main reaction layer and the transverse disturbance wavelength is long compared to the hydrodynamic thickness of the main reaction layer, this

layer may be approximated by a standard Rankine-Hugoniot discontinuity with heat addition. The Rankine-Hugoniot relations relate the gasdynamic state at the entrance to the main reaction layer to the outflow in the burnt zone (2.20). The general weakly nonlinear problem is then solved by integrating equations (2.13) subject to shock conditions (2.16) to determine the state at the entrance to the main reaction layer, and matching this behaviour across the main reaction layer to the sonic outflow condition in the burnt zone. In general this has to be done numerically, although an analytical solution is possible in characteristic form by invoking the Newtonian limit in which the specific heats ratio $\gamma \to 1$. This will be reported on in a future article. For the present, our concern is with the corresponding linear stability analysis of this weakly nonlinear system, though the preceding analysis has shown how the dynamics of a generalised two-dimensional mean-flow version of the Clarke equation is crucial to the understanding of the nonlinear problem of cellular detonation instability.

3. Linear stability analysis

The linear stability of the steady detonation wave solution $\mathbf{z}^*(x)$ to two-dimensional perturbations is determined from (2.13) in the preceding analysis by expanding $\hat{\mathbf{z}}$ as

$$\hat{\mathbf{z}} = \mathbf{z}_1^*(x) + \tilde{\mathbf{z}}(x,y,t), \quad \hat{h} = \tilde{h}, \tag{3.1}$$

where $\mathbf{z}_1^*(x)$ represents the $O(\theta^{-1})$ steady state solution in the induction zone, and the superscript $\tilde{}$ denotes a small linear perturbation quantity. Using (2.13) and (3.1), the linear stability problem becomes,

$$\tilde{\mathbf{z}}_{,t} + \mathbf{A}_0^* \cdot \tilde{\mathbf{z}}_{,x} + \mathbf{B}_0^* \cdot \tilde{\mathbf{z}}_{,y} = (\mathbf{C}_{ch})_0^* \cdot \tilde{\mathbf{z}}. \tag{3.2}$$

The $O(\theta^{-1})$ steady solution is found by substituting (3.1) into (2.2), giving

$$\mathbf{A}_0^* \cdot \mathbf{z}_{1,x}^* = \mathcal{K}\mathbf{c}_1^* e^{T_1^*}. \tag{3.3}$$

With null initial conditions at $x = 0$, the solution for $\mathbf{z}_1^*$ can be shown to be

$$\mathbf{z}_1^* = \left[-\frac{1}{(\gamma M_s^2 - 1)},\ \frac{M_s}{(\gamma M_s^2 - 1)},\ 0,\ -\frac{M_s^2}{(\gamma M_s^2 - 1)},\ -1,\ \frac{(M_s^2 - 1)}{\beta(\gamma M_s^2 - 1)}\right]^{\mathrm{T}} \ln(1-x). \tag{3.4}$$

The matrix $(\mathbf{C}_{ch})_0$ can then be written as

$$(\mathbf{C}_{ch})_0^*(x) = -\frac{\mathcal{K}}{\beta(1-x)} \begin{bmatrix} 0 & 0 & 0 & 0 & 0 & 0 \\ 0 & 0 & 0 & 0 & 0 & 0 \\ 0 & 0 & 0 & 0 & 0 & 0 \\ 0 & 0 & 0 & 0 & -\beta & 0 \\ 0 & 0 & 0 & 0 & -\gamma\beta & 0 \\ 0 & 0 & 0 & 0 & 1 & 0 \end{bmatrix}, \tag{3.5}$$

which depends on the spatially-varying steady induction zone structure, and reflects the singular nature of this structure near the main reaction layer. Elimination of $\tilde{\rho}$, $\tilde{u}$, $\tilde{v}$ and $\tilde{p}$ from (3.2) leads to an equation for $\tilde{T}$ in the form

$$[\partial_{,t} + M_s\partial_{,x}]\left([\partial_{,t} + M_s\partial_{,x}]^2\,\tilde{T} - \nabla^2\tilde{T}\right) \\ -\gamma\left([\partial_{,t} + M_s\partial_{,x}]^2\left[\frac{\tilde{T}}{1-x}\right] - \frac{1}{\gamma}\nabla^2\left[\frac{\tilde{T}}{1-x}\right]\right) = 0. \tag{3.6}$$

This is simply a linearised version of the mean-flow Clarke equation (2.14).

The system (3.2) is solved by first introducing a normal-mode decomposition for $\tilde{\mathbf{z}}$ and $\tilde{h}$ in the form

$$\tilde{\mathbf{z}} = \mathbf{z}'(x)e^{\lambda t + \mathrm{i}ky}, \quad \tilde{h} = h'e^{\lambda t + \mathrm{i}ky}, \tag{3.7}$$

with the complex growth rate given by λ, where $\mathrm{Re}(\lambda)$ defines the real growth rate, $\mathrm{Im}(\lambda)$ the frequency and k the wavenumber of the disturbance. The matrix $\mathbf{z}'(x)$ describes the spatial structure of the perturbation eigenfunctions in the displaced flow. The system (3.2) and shock conditions (2.16) become

$$\mathbf{A}_0^* \cdot \mathbf{z}'_{,x} + (\lambda + \mathrm{i}k\mathbf{B}_0^* - (\mathbf{C}_{ch})_0^*) \cdot \mathbf{z}' = 0 \tag{3.8}$$

and

$$\rho' = \lambda\kappa_\rho, \quad u' = \lambda\kappa_u, \quad v' = \mathrm{i}k\kappa_v, \quad p' = \lambda\kappa_p, \quad T' = \lambda(\gamma-1)\kappa_T, \quad Y' = 0. \tag{3.9}$$

This is precisely the linear system derived in Short & Stewart (1997). In order to solve the differential-matrix system (3.8) and (3.9) analytically, Short & Stewart (1997) invoke the additional assumption of the Newtonian limit, where

$$\theta^{-1} \ll (\gamma-1) \ll 1, \quad \mathbf{z}'(x) = \mathbf{z}'_0(x) + (\gamma-1)\mathbf{z}'_1(x) + \cdots, \tag{3.10}$$

in which the ordered limit between $(\gamma-1)$ and θ^{-1} is to be noted. Substituting, the system (3.8) is then solved sequentially for $\mathbf{z}'_0$ and $\mathbf{z}'_1$ to determine the perturbed induction zone solution. The result of this analysis is that the main reaction layer is found to be perturbed from its steady location $X = 1$ to a new location

$$X = F(y,t) \sim 1 + \widehat{F}'_0 e^{\lambda t + \mathrm{i}ky}, \tag{3.11}$$

where

$$\widehat{F}'_0 = h' - \theta(\gamma-1)\alpha, \tag{3.12}$$

with $\alpha \propto h'$ and a function of λ and k. Immediately in front of the main reaction layer, i.e. at $X = F^-(y,t)$, the matrix $\mathbf{z}'$ can be shown to have the value

$$\mathbf{z}'\{X = F^-(y,t)\} = \mathbf{z}'_F = [\rho'_F,\ u'_F,\ v'_F,\ p'_F,\ T'_F,\ Y'_F]^T, \tag{3.13}$$

where the $\{\ \}'_F$s are given explicitly in Short & Stewart (1997) as complicated functions of λ and k.

(*a*) *Main reaction layer jump, sonic flow and compatibility condition*

The perturbed linear flow in the burnt zone is determined by the expansion

$$\mathbf{z}_b = \mathbf{z}_b^* + \tilde{\mathbf{z}}_b(x,y,t), \tag{3.14}$$

where $\mathbf{z}_b^*$ represents the constant flow state in the burnt zone. When the outflow from the rear of the main reaction layer is locally sonic, i.e. for a Chapman-Jouguet detonation wave, a natural degeneracy in the description of $\tilde{\mathbf{z}}_b(x,y,t)$ appears (Short & Stewart 1997), in which the upstream propagating acoustic waves are eliminated. In such circumstances, the perturbed flow solution in the burnt zone must satisfy the normal-mode linear compatibility condition

$$\lambda u_b' - ik\nu_b v_b' - \frac{\lambda p_b'}{\mu_b \nu_b} = 0. \tag{3.15}$$

The quantities ν_b and μ_b represent the ratios of the frozen sound speed and density in the uniform steady burnt state to those immediately behind the steady detonation shock, and for a given Chapman-Jouguet detonation velocity D_{CJ}, their values are given in appendix A.

As noted previously, the analysis in Short & Stewart (1997) is valid for disturbances that are of sufficiently low frequency and long wavelength that the main reaction layer can be treated as a Rankine-Hugoniot discontinuity. This has an important implication, namely that for sufficiently large activation energies the disturbance frequencies can then be significantly lower and wavelengths significantly longer than the appropriate scales defined by the induction zone. It is this property that is exploited below to derive simplified polynomial forms of the dispersion relation obtained in Short & Stewart (1997). For the generalised scales in Short & Stewart, the Rankine-Hugoniot relations are used to relate the perturbation quantities at $X = F^-(y,t)$ to those at the rear of the main reaction layer, where

$$\bar{\mathbf{z}} = \mathbf{z}_b'\{X = F^+(y,t)\}e^{\lambda t + iky} \tag{3.16}$$

For general detonation velocities, i.e. for $M_b \leq 1$, where M_b is the steady Mach number in the burnt zone, the three Rankine-Hugoniot jumps can be represented in matrix form as

$$\mathbf{A}_b^* \cdot \mathbf{e}_b' = \mathbf{a}_\rho^* \rho_F' + \mathbf{a}_u^* u_F' + \mathbf{a}_p^* p_F' + \mathbf{a}_Y^* Y_F' + \mathbf{A}_{\widehat{F}}^* \widehat{F}_0', \tag{3.17}$$

where

$$\mathbf{e}_b' = \begin{bmatrix} \rho_b' \\ u_b' \\ p_b' \end{bmatrix}, \quad \mathbf{A}_{\widehat{F}}^* = \begin{bmatrix} \mu_b - 1 \\ 0 \\ (\gamma-1)(M_b\nu_b - M_s) \end{bmatrix}, \tag{3.18}$$

and

$$\mathbf{a}_\rho = \begin{bmatrix} M_s \\ M_s^2 \\ -1 \end{bmatrix}, \quad \mathbf{a}_u = \begin{bmatrix} 1 \\ 2M_s \\ (\gamma-1)M_s \end{bmatrix}, \quad \mathbf{a}_p = \begin{bmatrix} 0 \\ 1 \\ \gamma \end{bmatrix}, \quad \mathbf{a}_Y = \begin{bmatrix} 0 \\ 0 \\ \beta \end{bmatrix}. \tag{3.19}$$

The matrix $\mathbf{A}_b^*$ is given by

$$\mathbf{A}_b^* = \begin{bmatrix} M_b\nu_b & \mu_b & 0 \\ \nu_b^2 M_b^2 & 2\mu_b\nu_b M_b & 1 \\ -\nu_b^2/\mu_b & (\gamma-1)M_b\nu_b & \gamma/\mu_b \end{bmatrix}, \tag{3.20}$$

and for $M_b = 1$ its inverse $(\mathbf{A}_b^*)^{-1}$ is singular. The singularity arises because $\mathbf{e}_b'$ must necessarily satisfy the the Chapman-Jouguet compatibility relation (3.15), when $M_b = 1$. The regularity condition on the four equations (3.17) and (3.15) is determined as

$$R_1 p_F' + R_2 u_F' + R_3 Y_F' + R_4 \rho_F' + \lambda R_5 \widehat{F}_0' = 0, \tag{3.21}$$

where

$$R_1 = \gamma\left(\frac{1}{\mu_b} - 1\right), \quad R_2 = \frac{\nu_b}{\mu_b}(\mu_b - 1)\left[\gamma + 1 - (\gamma-1)\mu_b\right], \quad R_3 = -\beta,$$
$$R_4 = \nu_b^2\left(\gamma\mu_b - (\gamma+1)\right) + 1, \quad R_5 = \frac{(\mu_b - 1)}{\mu_b}\nu_b\left[-(\gamma+1) + (\gamma-1)\mu_b\right]. \tag{3.22}$$

This determines the dispersion relation governing the stability of Chapman-Jouguet detonations in the limit of large activation energy. Although the matrix $\mathbf{z}_F'$ is a complex function of λ and k the analysis is valid for a disturbance frequency that is small on the inverse time-scale of particle passage through the main reaction layer, and a transverse disturbance wavelength that is long compared to the hydrodynamic thickness of the main reaction layer. Due to its complexity, the dispersion relation has to solved numerically in general, and this has been done in Short and Stewart (1997). Excellent qualitative agreement with the behaviour of exact numerical solutions of the detonation stability problem was obtained.

In the following work, additional low-frequency and long-wavelength limits on scales associated with induction zone quantities will be exploited, i.e., in circumstances where

$$\lambda = O(\delta), \quad k = O(\delta) \quad \text{or} \quad k = O(\sqrt{\delta}), \quad \delta \ll 1. \tag{3.23}$$

In this manner it is possible to derive straightforward explicit polynomial expressions for the dispersion relation and analyse the properties of the corresponding linear evolution equations in order to understand the initial dynamics of cellular detonation formation.

4. Low-frequency pulsating instability

Numerical simulations of nonlinear one-dimensional detonation instability reveal a pulsating behaviour of the front. The frequency of the pulsation is found to be low on the scale of the inverse particle transit time through the detonation induction zone (Abouseif & Toong 1982; Bourlioux, Majda & Roytburd 1991; Quirk 1994), and moreover, for regimes in which there is a single unstable mode in the linear stability spectra, the frequency of the fully nonlinear pulsation is almost identical to that associated with the frequency of the linear mode. As noted

by Abouseif & Toong 1982, this indicates that the salient features of the nonlinear pulsating instability mechanism are captured by the dynamics associated with the low-frequency unstable linear mode. For planar disturbances ($k = 0$), an explicit polynomial expression for the low-frequency mode can be obtained from the dispersion relation (3.21) when

$$\lambda = O(\delta), \quad \delta \ll 1. \tag{4.1}$$

The functions $\mathbf{z}'_F$ can then be expanded in algebraic powers of λ in a straightforward manner and the third-order polynomial dispersion relation

$$(\theta(\gamma-1)C_5 + C_6)\,\lambda^3 + (\theta(\gamma-1)C_2 + C_3)\,\lambda^2 + C_1\lambda = 0 \tag{4.2}$$

derived, after truncating the expansion so that terms up to $O(\delta^3)$ are retained. The coefficients C_i depend on the post-shock flow Mach number M_s, the heat release β and the ratio of specific heats γ, and are given explicitly in appendix B. The terms involving the product $\theta(\gamma-1)$ are generated by the displacement of the fire-zone relative to the shock front. The corresponding one-dimensional linear evolution equation for $\tilde{h}$ (3.7) is given by the third-order equation

$$A_4 h_{,ttt} + A_2 h_{,tt} + A_1 h_{,t} = 0, \tag{4.3}$$

where the tilde on $\tilde{h}$ has been dropped, and where,

$$A_1 = C_1, \quad A_2 = \theta(\gamma-1)C_2 + C_3, \quad A_4 = \theta(\gamma-1)C_5 + C_6. \tag{4.4}$$

Figure 1 shows the variation of A_1, A_2 and A_4 in the activation energy E - heat release Q plane for realistic variations in the parameters $5 < Q < 30$ and $5 < E < 30$. The non-dimensional quantities E and Q represent detonation velocity independent scalings, and their relation to θ and β is given in appendix A. Thus, in these regimes we have both $A_1 < 0$ and $A_4 < 0$, whereas A_2 can be either positive or negative depending on the relative values of Q and E. Figure 2 shows the variation of A_1, A_2 and A_4 with E for $Q = 10$ and $Q = 20$.

The second-order evolution equation and dispersion relation obtained by truncating the expansion at $O(\delta^2)$,

$$A_2 h_{,tt} + A_1 h_{,t} = 0, \quad A_2\lambda^2 + A_1\lambda = 0, \tag{4.5}$$

is the Chapman-Jouguet equivalent of that derived previously by Buckmaster & Ludford (1986) for overdriven waves. The dispersion relation consists of the null eigenvalue and the single real eigenvalue

$$\lambda = -\frac{A_1}{A_2}. \tag{4.6}$$

Since $A_1 < 0$, the real root is stable in regimes where $A_2 < 0$ and unstable where $A_2 > 0$. Figure 3 shows the variation of the unstable eigenvalue (4.6) with activation energy E for $Q = 10$. A singularity in the growth rate occurs when $A_2 = 0$. Buckmaster (1988) has shown that the slowly-varying nonlinear evolution equation corresponding to the unstable regime of the linear evolution equation (4.5) leads to a situation where the induction zone either collapses or lengthens indefinitely. Additionally, Short (1997) has shown that such low-frequency real roots do occur in the actual linear stability spectra, but only in the limit of unrealistically large activation energy. More complex models must therefore be

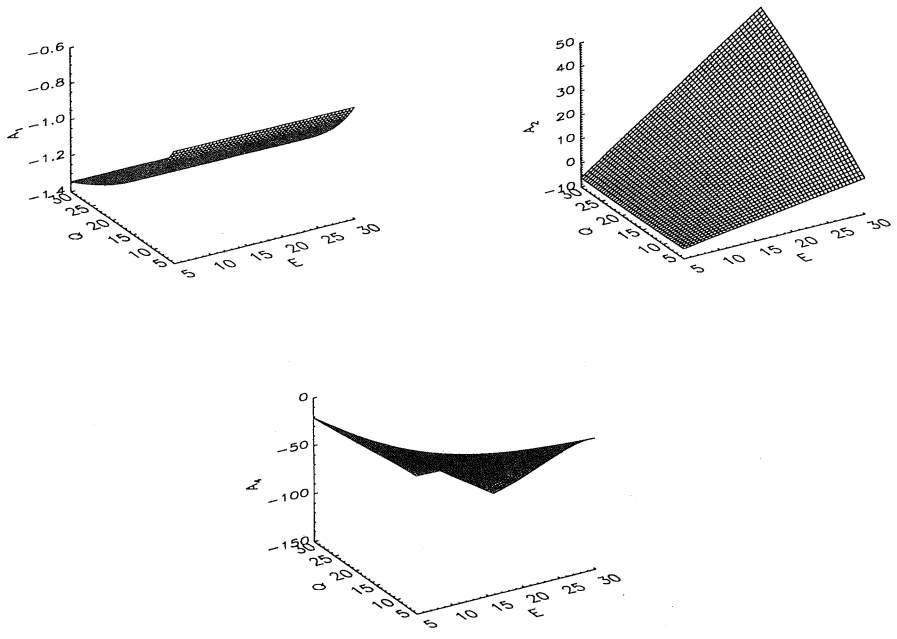

Figure 1. The variation of A_1, A_2 and A_4 in the E - Q plane for $\gamma = 1.1$.

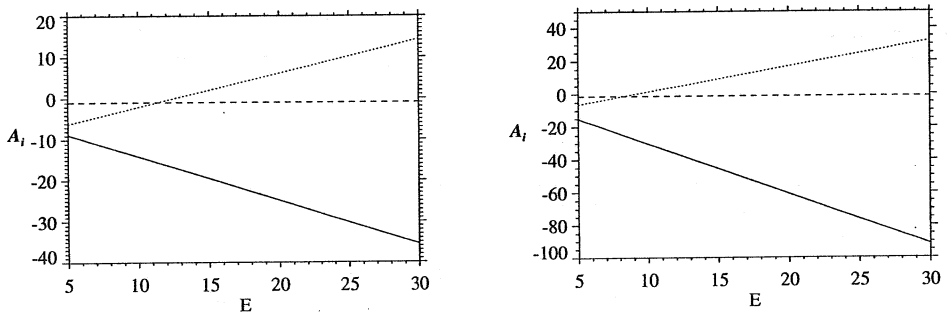

Figure 2. The variation of A_1 (dashed line), A_2 (dotted line) and A_4 (solid line) with E for $\gamma = 1.1$ and (a) $Q = 10$ (b) $Q = 20$.

sought to describe the general stability problem, and this occurs in the form of the third-order evolution equation (4.3).

The dispersion relation corresponding to (4.3) is given by

$$A_4\lambda^3 + A_2\lambda^2 + A_1\lambda = 0, \tag{4.7}$$

and represents a forced, $A_2 > 0$, or damped, $A_2 < 0$, linear oscillator. The linear system is similar to that derived by Yao & Stewart (1996) but with an additional term appearing in the coefficient of λ^3. Apart from $\lambda = 0$, the equation (4.7) has the roots

$$\lambda = -\frac{A_2}{2A_4} \pm \frac{1}{2A_4}\left(A_2^2 - 4A_4A_1\right)^{1/2}. \tag{4.8}$$

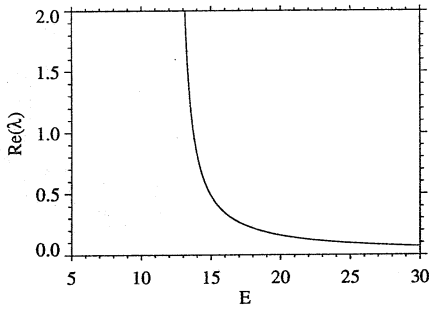

Figure 3. The variation of $\mathrm{Re}(\lambda)$ with E from (4.6) for $\gamma = 1.1$ and $Q = 10$.

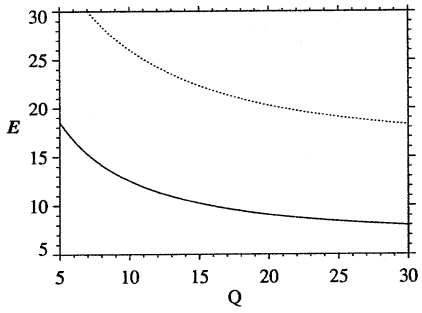

Figure 4. The neutral stability curve (solid line) and bifurcation curve (dotted line) between purely real and oscillatory roots in Q - E space from (4.8) for $\gamma = 1.1$. The region to the left of the solid curve is stable, and between the curves, the root is oscillatory.

Since $A_1 A_4 > 0$, the root is neutrally stable when $A_2 = 0$, but in contrast to the second-order equation (4.5) it is not degenerate along $A_2 = 0$. An oscillatory unstable root is present when $A_2^2 < 4A_1A_4$ and $A_2 > 0$ and two purely real unstable roots when $A_2^2 > 4A_1A_4$ and $A_2 > 0$. Figure 4 shows the neutral stability curve $A_2 = 0$ in the Q - E plane and the bifurcation curve $A_2^2 = 4A_1A_4$ between oscillatory and non-oscillatory modes, as predicted by (4.8). The region to the right of the solid line is unstable, with the root being oscillatory to the left of the dotted line.

Figure 5 shows the behaviour of the growth rate $\mathrm{Re}(\lambda)$ and frequency $\mathrm{Im}(\lambda)$ with activation energy E for $Q = 10$ of the unstable mode as predicted from (4.8). Also shown is a comparison with the corresponding root calculated from the dispersion relation (3.21). There is a bifurcation point at $E = 12.5$ rendering the oscillatory mode linearly unstable. The frequency decays as the growth rate increases until a bifurcation to two real roots occurs at $E = 26.0$. The lower real root corresponds to that calculated from the second-order equation (4.5).

The third-order linear evolution equation (4.3) thus contains all of the properties associated with the linear dynamics of a pulsating detonation front, and should therefore be a good qualitative model for understanding the onset of one-dimensional detonation instability. In particular, Buckmaster & Ludford (1986) have shown that the second-order equation (4.5) occurs when the level of approximation is such that perturbations at the shock propagate through the induction

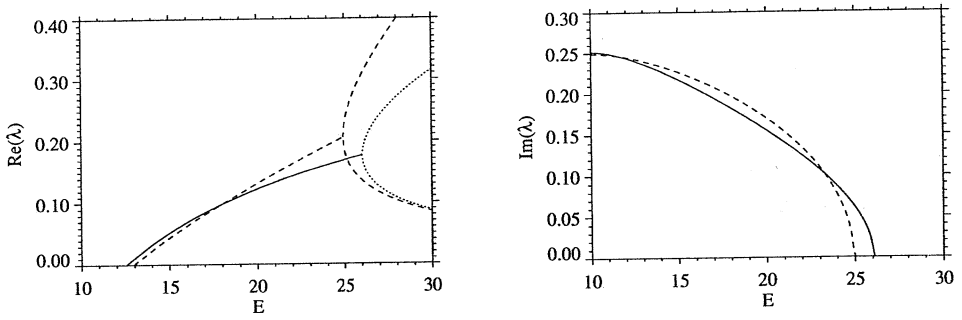

Figure 5. The behaviour of $\mathrm{Re}(\lambda)$ and $\mathrm{Im}(\lambda)$ with E from (4.8) for $\gamma = 1.1$ and $Q = 10$. The dotted line represents real roots. The dashed line is from Short & Stewart (1997).

zone in a quasi-steady manner, so that the disturbances are propagated along entropy paths only. The third-order system results from the inclusion of higher-order acoustic wave propagation in the induction zone. Importantly, information about the fire-zone perturbation is now propagated back to the shock-front and this gives rise to the oscillatory mechanism of instability.

5. Cellular instability - Hyperbolic evolution $\lambda = O(k)$

When detonation waves propagate in a rectangular tube, they exhibit a striking form of cellular instability. Recent numerical simulations (Bourlioux & Majda 1992; Quirk 1994; Williams, Bauwens & Oran 1996) have been able to capture most of the salient features of the cellular instability mechanism. Bourlioux and Majda (1992) have also found that in a regime where there is a single unstable two-dimensional mode in the linear stability spectrum, a very regular cell pattern is formed, whose initial cell size correlates well with the wavelength associated with the maximum growth rate of the unstable mode. Yao and Stewart (1996) have recently proposed that the cellular instability can be modelled by a nonlinear evolution equation based on the limits of near Chapman-Jouguet detonation velocity, large dimensionless activation energy, long-wavelength shock perturbations on the scale of the induction zone thickness and slow dynamic shock evolution measured on the time scale of particle passage through the induction zone. Stewart *et al.* (1996) have shown that the corresponding linear evolution is third-order in time and second-order in space and consists of a sequence of hyperbolic wave operators. A similar hyperbolic linear evolution equation can be derived from (3.21) in situations where

$$\lambda = O(\delta), \quad k = O(\delta). \tag{5.1}$$

The polynomial dispersion relation derived by expanding (3.21) under these limits for $\delta \ll 1$ is given by

$$\begin{aligned} &C_1\lambda + \left[\{\theta(\gamma-1)C_2 + C_3\}\,\lambda^2 + C_4k^2\right] \\ &+\lambda\left[\{\theta(\gamma-1)C_5 + C_6\}\,\lambda^2 + \{\theta(\gamma-1)C_7 + C_8\}\,k^2\right] = 0, \end{aligned} \tag{5.2}$$

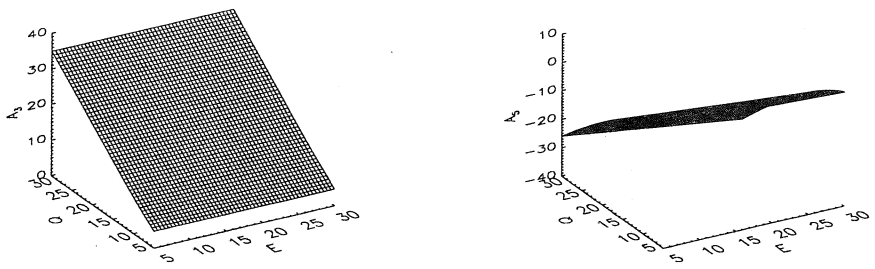

Figure 6. The variation of A_3 and A_5 in the Q - E plane for $\gamma = 1.1$.

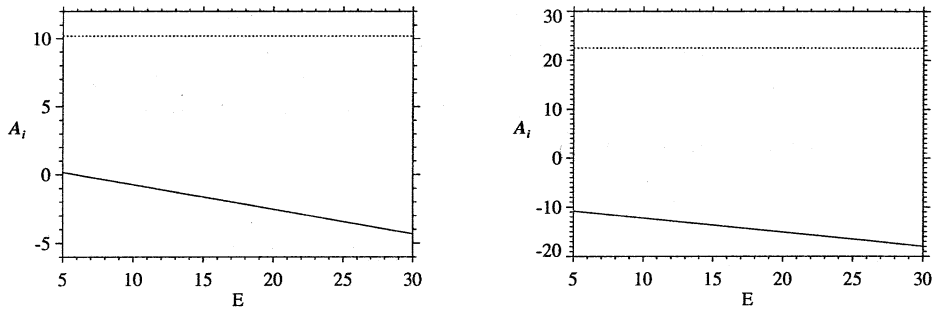

Figure 7. The variation of A_3 (dotted line) and A_5 (solid line) with E for $\gamma = 1.1$ and (a) $Q = 10$ (b) $Q = 20$.

after truncating the expansion so that terms up to $O(\lambda^3, \lambda k^2)$ have been retained. The corresponding two-dimensional linear evolution equation is given by

$$[A_4 h_{,tt} + A_5 h_{,yy}]_{,t} + [A_2 h_{,tt} + A_3 h_{,yy}] + A_1 h_{,t} = 0, \tag{5.3}$$

which is third-order in time and second-order in space and where,

$$A_3 = -C_4, \quad A_5 = -\left(\theta(\gamma - 1)C_7 + C_8\right). \tag{5.4}$$

Equation (5.3) consists of a sequence of operators, which depending on the signs of A_2, A_3, A_4 and A_5 can be either elliptic or hyperbolic. Figure 6 shows the variation of A_3 and A_5 in the E - Q plane, and for the parameter regime shown, $A_3 > 0$, whereas A_5 can be either positive or negative. Figure 7 shows the variation of A_3 and A_5 with E for $\gamma = 1.1$ and $Q = 10$ and $Q = 20$.

The second-order system,

$$[A_2 h_{,tt} + A_3 h_{,yy}] + A_1 h_{,t} = 0 \tag{5.5}$$

is obtained by retaining terms up to $O(\lambda^2, k^2)$ and corresponds to the well-known linear telegraph equation. Buckmaster & Ludford (1986) find that curvature of the detonation front plays no role in defining the induction zone structure at this order. Since $A_3 > 0$, the equation is hyperbolic if $A_2 < 0$ and elliptic if $A_2 > 0$. For Cauchy type initial data, the equation is therefore ill-posed for $A_2 > 0$ in the sense that the positive growth rate increases monotonically with wavenumber k.

For $A_2 < 0$, the dispersion relation corresponding to (5.5) has the solution

$$\lambda = -\frac{A_1}{2A_2} \pm \frac{1}{2}\sqrt{\left(\frac{A_1}{A_2}\right)^2 + 4\left(\frac{A_3}{A_2}\right)k^2}, \tag{5.6}$$

corresponding to two negative real roots for

$$k^2 < k_c^2 = \left(\frac{A_1}{A_2}\right)^2 \Big/ 4\left(\frac{A_3}{A_2}\right), \tag{5.7}$$

and a complex-conjugate root for

$$k^2 > k_c^2, \tag{5.8}$$

with dissipation rate

$$\lambda = -\frac{1}{2}\left(\frac{A_1}{A_2}\right). \tag{5.9}$$

Merging of the real roots into the oscillatory root occurs at $k = k_c$. Thus a well-posed second-order linear evolution equation occurs only when the modes have negative growth rates and a higher-order system is clearly required to describe the two-dimensional instability.

The third-order evolution equation (5.3), on the other hand, includes higher-order acoustic effects in the induction zone. The corresponding dispersion relation is

$$\lambda^3 + \frac{A_2}{A_4}\lambda^2 + \frac{1}{A_4}\left(A_1 - A_5k^2\right)\lambda - \frac{A_3}{A_4}k^2 = 0. \tag{5.10}$$

For the Q - E regimes of interest $A_3 > 0$, $A_1 < 0$ and $A_4 < 0$, whereas A_2 and A_5 can be either positive or negative. Since $A_3/A_4 < 0$, the cubic (5.10) always has one real root with a negative growth rate. In the limit $k \to \infty$, $\lambda \sim \alpha_0 k + \alpha_1$, where

$$\alpha_0^2 = \frac{A_5}{A_4}. \tag{5.11}$$

Since $A_4 < 0$, we require $A_5 > 0$ and α_0 purely imaginary, for (5.3) to be a well-posed linear evolution equation. This has the additional implication that the highest-order operator in (5.3) be hyperbolic. At the next order, α_1 is determined as

$$\alpha_1 = \frac{A_4}{2A_5}\left(\frac{A_3}{A_4} - \frac{A_2A_5}{A_4^2}\right). \tag{5.12}$$

Having determined that $A_5/A_4 < 0$ for a well-posed solution, it is now required that

$$\left(\frac{A_3}{A_4} - \frac{A_2A_5}{A_4^2}\right) > 0 \tag{5.13}$$

for the dispersion relation to have modes with negative decay rates as $k \to \infty$. This condition ensures that there is some critical wavenumber above which the evolution equation (5.3) is stable.

In contrast, global stability to two-dimensional disturbances of the cubic (5.10) requires both

$$\frac{A_2}{A_4} > 0, \quad -\frac{A_3}{A_4} > 0 \tag{5.14}$$

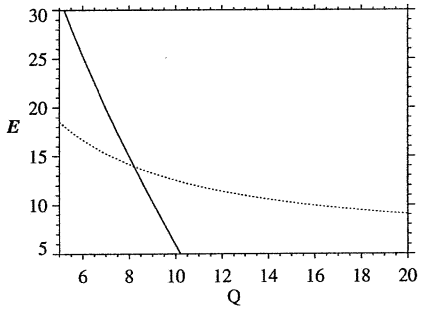

Figure 8. The region to the left of the solid line $A_5 = 0$ determines the regime of well-posed solutions for equation (5.3) with $\gamma = 1.1$. Also shown is the one-dimensional neutral stability curve (dotted line) from (4.8).

and

$$\left(\frac{A_3}{A_4} - \frac{A_2 A_5}{A_4^2}\right) k^2 + \frac{A_2 A_1}{A_4^2} > 0. \tag{5.15}$$

The former requires $A_2 < 0$, and since $A_2 A_1 > 0$, two-dimensionally stable solutions occur in regions where

$$\left(\frac{A_3}{A_4} - \frac{A_2 A_5}{A_4^2}\right) > 0. \tag{5.16}$$

But this is precisely the condition (5.13) required for negative growth rates as $k \to \infty$; in other words, when the system is well-posed but unstable to two-dimensional disturbances, the growth rate as $k \to \infty$ is constant but positive. This rules out the existence of stable solutions for sufficiently large k. It can also be shown that when the above criteria for well-posed solutions are met, the growth rate predicted by the cubic (5.10) will not possess a local maximum in wavenumber space. These are the two properties required for the extension of the analysis of Yao & Stewart (1996). Figure 8 shows the regimes of E - Q space for $\gamma = 1.1$ in which the cubic evolution equation has well-posed solutions. Figure 9 shows the behaviour of the growth rate and frequency of the unstable oscillatory mode which arises in (5.10) when $Q = E = 7.5$ and $\gamma = 1.1$. Also shown is the corresponding mode calculated from (3.22). The cubic equation is only a good approximation for the growth rate for very small k and does not possess a maximum for any value of k, tending to a limiting value $\mathrm{Re}(\lambda) = 2.3$ as $k \to \infty$. In order to overcome the limitations of the lack of a maximum growth rate and stability for sufficiently large wavenumbers, we turn to the strategy adopted by Buckmaster (1989) and derive a generalised parabolic evolution equation for cellular detonation instability.

6. Cellular instability - Parabolic evolution $\lambda = O(k^2)$

In order to overcome the deficiencies of Buckmaster and Ludford (1986), Buckmaster (1989) introduced a modified scaling for disturbance wavelength. Specifically, Buckmaster (1989) is concerned with a long-wavelength perturbation which varies on the scale of the inverse square root of the perturbation frequency identified in Buckmaster and Ludford (1986). This analysis recovers a single real root

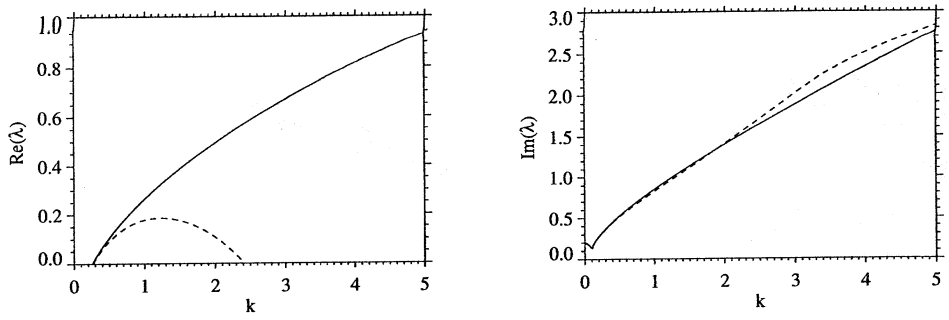

Figure 9. The behaviour of Re(λ) and Im(λ) with k from (5.10) for $E = 7.5$, $Q = 7.5$ and $\gamma = 1.1$. The dashed line is the corresponding root from (3.21). In the limit $k \to \infty$, Re(λ) $\to$ 2.3.

with a maximum growth rate in wavenumber space. Importantly, curvature of the detonation front now plays a role in the induction zone dynamics. However, Short (1997) has found that the activation energy has to be unrealistically large in order to recover this asymptotic stability behaviour from the exact linear stability problem, and higher-order terms must be included in the description of the linear dispersion relation. These terms can be obtained directly from (3.21).

With scales for λ and k such that $\lambda = O(\delta)$ and $k = O(\sqrt{\delta})$, $\delta \ll 1$, the dispersion relation (3.21) can be expanded and truncated to retain terms up to $O(\delta^3)$, resulting in the polynomial dispersion relation

$$\begin{aligned}&\left[C_1\lambda + C_4k^2\right] + \left[\{\theta(\gamma-1)C_2 + C_3\}\lambda^2 + \{\theta(\gamma-1)C_7 + C_8\}\lambda k^2 + C_{13}k^4\right]\\ &+ \left[\{\theta(\gamma-1)C_5 + C_6\}\lambda^3 + \{\theta(\gamma-1)C_{11} + C_{12}\}\lambda^2k^2\right.\\ &\left.+ \{\theta(\gamma-1)C_{18} + C_{19}\}\lambda k^4 + C_{20}k^6\right] = 0.\end{aligned} \tag{6.1}$$

The corresponding dispersive linear evolution equation is

$$\begin{aligned}&[A_4h_{,ttt} + A_7h_{,yytt} + A_{11}h_{,yyyyt} + A_{12}h_{,yyyyyy}]\\ &+ [A_2h_{,tt} + A_5h_{,yyt} + A_8h_{,yyyy}] + A_1h_{,t} + A_3h_{,yy} = 0,\end{aligned} \tag{6.2}$$

which is third-order in time and sixth-order in space. The coefficients A_7, A_8, A_{11} and A_{12} are given by

$$\begin{aligned}&A_7 = -\left(\theta(\gamma-1)C_{11} + C_{12}\right), \quad A_8 = C_{13},\\ &A_{11} = \theta(\gamma-1)C_{18} + C_{19}, \quad A_{12} = -C_{20},\end{aligned} \tag{6.3}$$

where the C_i's are given in appendix B. Figure 10 shows the variation of A_7, A_8, A_{11} and A_{12} in the Q - E plane, and for the parameter regimes shown, $A_7 > 0$, $A_8 < 0$, $A_{12} > 0$, whereas A_{11} can be either positive or negative. Figure 11 shows the variation of A_7, A_8, A_{11} and A_{12} with E for two values of the heat release Q. The linear evolution equation (6.2) consists of a sequence of three dispersive parabolic wave operators and below we will investigate the various physical properties of each order of the evolution equation. This leads to the main result of the paper; namely that the third-order temporal equation (6.2) encapsulates all the major properties of the linear dispersion relation corresponding to two-dimensional detonation wave stability.

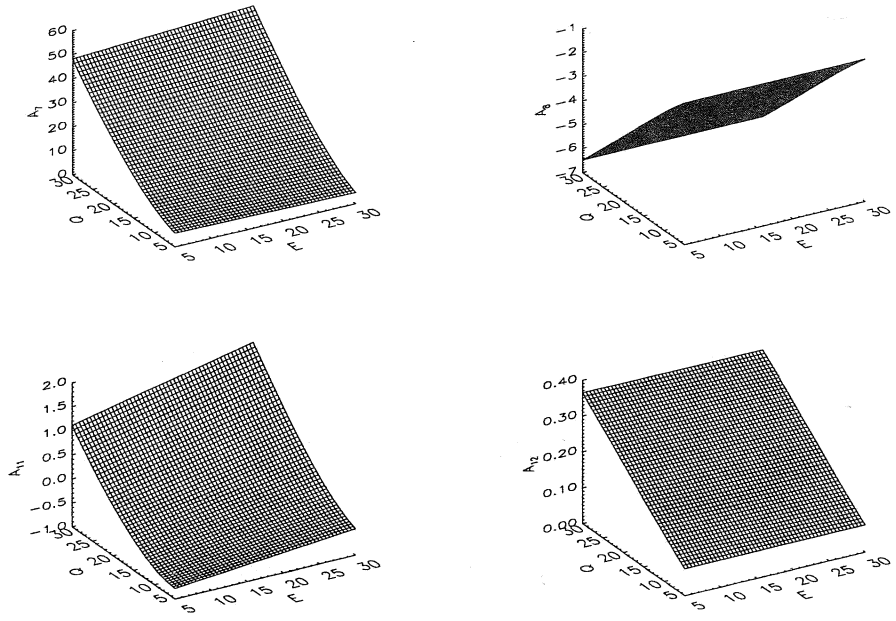

Figure 10. (a) The variation of A_7, A_8, A_{11} and A_{12} in the E - Q plane for $\gamma = 1.1$.

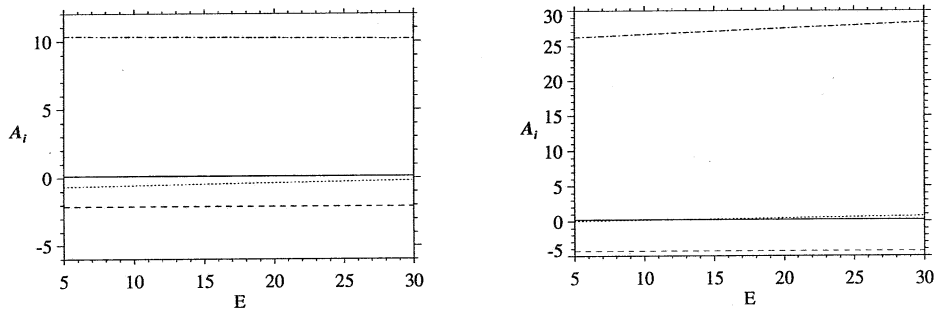

Figure 11. The variation of A_7 (dash-dot), A_8 (dash), A_{11} (dot) and A_{12} (solid) with E for $\gamma = 1.1$ and (a) $Q = 10$ (b) $Q = 20$.

The lowest-order evolution equation and corresponding dispersion relation are

$$A_1 h_t + A_3 h_{yy} = 0, \quad A_1 \lambda - A_3 k^2 = 0 \tag{6.4}$$

respectively, which is first-order in time and second-order in space. This is simply the parabolic heat equation, with dispersion relation solution

$$\lambda = \frac{A_3}{A_1} k^2. \tag{6.5}$$

Since $A_1 < 0$ and $A_3 > 0$, the equation (6.4) is well-posed with the dispersion relation having one real root with a negative growth rate $\forall k$.

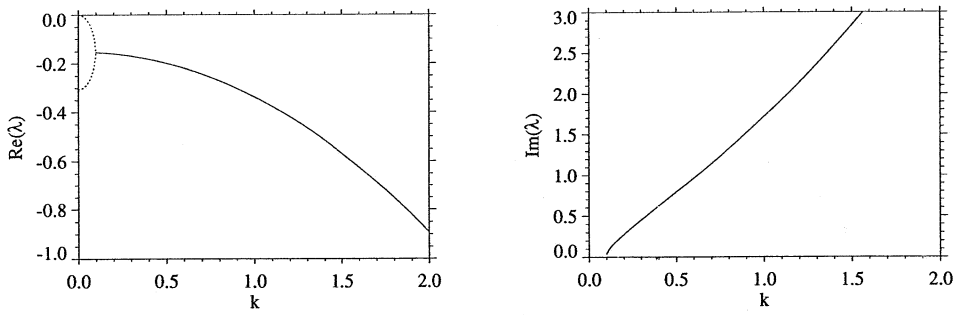

Figure 12. (a) The variation of $\mathrm{Re}(\lambda)$ and $\mathrm{Im}(\lambda)$ from (6.7) with $Q = 10$, $E = 10$, and $\gamma = 1.1$. The dotted lines represent non-oscillatory roots.

At the next order of approximation, the linear evolution equation is given by

$$[A_2 h_{,tt} + A_5 h_{,yyt} + A_8 h_{,yyyy}] + [A_1 h_{,t} + A_3 h_{,yy}] = 0, \tag{6.6}$$

which is second-order in time and fourth-order in space, and consists of two dispersive wave operators with dispersion relation

$$A_2\lambda^2 + \left(A_1 - A_5 k^2\right)\lambda - A_3 k^2 + A_8 k^4 = 0. \tag{6.7}$$

In the limit $k \to \infty$, $\lambda \sim \alpha k^2$, where α satisfies

$$A_2\alpha^2 - A_5\alpha + A_8 = 0. \tag{6.8}$$

Since $A_8 < 0$, we must have

$$A_2 < 0, \quad A_5 > 0 \tag{6.9}$$

for a well-posed equation in which $\mathrm{Re}(\alpha) < 0$ as $k \to \infty$. Also, since $-A_3 k^2 + A_8 k^4 < 0\ \forall k$, general stability to two-dimensional disturbances occurs in regimes where

$$A_1 - A_5 k^2 < 0. \tag{6.10}$$

From (6.9) $A_5 > 0$, and given $A_1 < 0$, the relation (6.10) is always satisfied and the well-posed second-order evolution equation (6.6) is stable to all two-dimensional disturbances. However, an important difference between (6.4) and (6.6) does occur, since an oscillatory stable root is now present when

$$\left(A_5^2 - 4A_2A_8\right)k^4 + \left(4A_2A_3 - 2A_1A_5\right)k^2 + A_1^2 < 0. \tag{6.11}$$

Since $A_8 < 0$, this must always be true for sufficiently large k when $4A_2A_8 > A_5^2$. In such circumstances, the two non-oscillatory modes present for $k = 0$ must merge into a single oscillatory mode at some critical wavenumber $k = k_c$. Figure 12 shows the behaviour of dissipation rate of the stable mode with k for $Q = 10$, $E = 10$ and $\gamma = 1.1$. The two non-oscillatory modes merge into a single oscillatory mode at $k = 0.1$.

(*a*) *Third-order problem*

By retaining terms up to $O(\delta^3)$, the resulting linear evolution equation (6.2) that is derived is third-order in time and sixth-order in space, consisting of a

sequence of three dispersive parabolic wave operators. The dispersion relation corresponding to (6.2) is

$$A_4\lambda^3+(A_2-A_7k^2)\lambda^2+(A_1-A_5k^2+A_{11}k^4)\lambda-A_3k^2+A_8k^4-A_{12}k^6=0. \quad (6.12)$$

Since $A_4<0$, $A_3>0$, $A_8<0$ and $A_{12}>0$, one result that immediately follows is that (6.12) must always possess one real negative root. In the limit $k\to\infty$, $\lambda\sim\alpha k^2$, where α satisfies

$$\alpha^3-\frac{A_7}{A_4}\alpha^2+\frac{A_{11}}{A_4}\alpha-\frac{A_{12}}{A_4}=0. \quad (6.13)$$

For the realistic parameter regimes we are concerned with, both $A_7/A_4<0$ and $A_{12}/A_4<0$, and thus well-posed regions where $\mathrm{Re}(\alpha)<0$ occur in regimes satisfying

$$-\frac{A_7}{A_4}\frac{A_{11}}{A_4}>-\frac{A_{12}}{A_4}, \quad (6.14)$$

which in turn is only possible when $A_{11}<0$. The dashed line in figure 13(a) shows the boundary to the left of which well-posed solutions of (6.2) are possible in the E - Q plane. Regimes which are stable to all two-dimensional disturbances occur when

$$\frac{1}{A_4}(A_2-A_7k^2)>0, \quad \forall k, \quad (6.15)$$

which requires $A_2<0$, and when

$$\left(\frac{A_2}{A_4}-\frac{A_7}{A_4}k^2\right)\left(\frac{A_1}{A_4}-\frac{A_5}{A_4}k^2+\frac{A_{11}}{A_4}k^4\right)>\left(-\frac{A_3}{A_4}k^2+\frac{A_8}{A_4}k^4-\frac{A_{12}}{A_4}k^6\right), \quad \forall k, \quad (6.16)$$

or rewriting, when

$$\begin{aligned}&\frac{A_1A_2}{A_4^2}+\left(-\frac{A_1A_7}{A_4^2}-\frac{A_5A_2}{A_4^2}+\frac{A_3}{A_4}\right)k^2\\&+\left(\frac{A_2A_{11}}{A_4^2}+\frac{A_5A_7}{A_4^2}-\frac{A_8}{A_4}\right)k^4+\left(-\frac{A_7}{A_4}\frac{A_{11}}{A_4}+\frac{A_{12}}{A_4}\right)k^6>0, \quad \forall k.\end{aligned} \quad (6.17)$$

If we further rewrite this in the form

$$k^6+lk^4+mk^2+n>0, \quad (6.18)$$

where

$$\begin{aligned}l &= \left(\frac{A_2A_{11}}{A_4^2}+\frac{A_5A_7}{A_4^2}-\frac{A_8}{A_4}\right)\left(-\frac{A_7}{A_4}\frac{A_{11}}{A_4}+\frac{A_{12}}{A_4}\right)^{-1},\\ m &= \left(-\frac{A_1A_7}{A_4^2}-\frac{A_5A_2}{A_4^2}+\frac{A_3}{A_4}\right)\left(-\frac{A_7}{A_4}\frac{A_{11}}{A_4}+\frac{A_{12}}{A_4}\right)^{-1},\\ n &= \frac{A_1A_2}{A_4^2}\left(-\frac{A_7}{A_4}\frac{A_{11}}{A_4}+\frac{A_{12}}{A_4}\right)^{-1},\end{aligned} \quad (6.19)$$

the regimes of two-dimensional stability occur when

$$27n^2-18nlm-l^2m^2+4l^3n+4m^3>0. \quad (6.20)$$

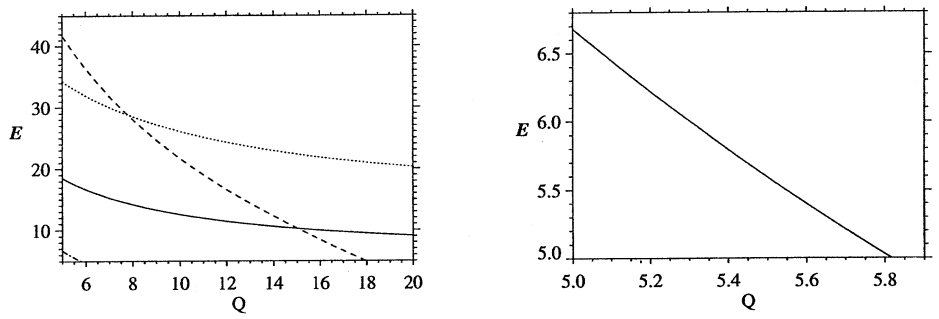

Figure 13. (a) Neutral stability curves and well-posed regions of detonation stability corresponding to the linear evolution equation (6.2) and dispersion relation (6.12). The region to the left of the dashed line corresponds to well-posed solutions, the region to the right of the dot-dash line to two-dimensional instability. The region to the right of the solid line corresponds to one-dimensional instability. The region to the right of the dotted line corresponds to one-dimensional non-oscillatory solutions. (b) The two-dimensional neutral stability curve in the Q-E plane.

Figure 13(b) shows the boundary in the E - Q plane to the left of which two-dimensional stability occurs. This is shown as the dot-dash line in figure 13(a). Thus in figure 13(a) the region to the right of the dot-dash line but to the left of the solid line is one-dimensionally stable, but has a finite band of unstable wavenumbers. The region to the right of the solid line corresponds to one-dimensional unstable regimes, but for regions to the left of the dashed line, stability prevails for sufficiently large k.

Figures 14 and 16 show the behaviour of the growth rate $\mathrm{Re}(\lambda)$ and frequency $\mathrm{Im}(\lambda)$ of the unstable mode present in the dispersion relation (6.12) for two cases lying either side of the one-dimensional neutral stability boundary. Figure 14 is for $Q = 10$, $E = 10$ and $\gamma = 1.1$ which is stable to one-dimensional disturbances. As the wavenumber increases, the two-dimensional oscillatory mode first becomes unstable at $k = 0.13$, and thereafter its growth rate increases monotonically with k before reaching a maximum at $k = 1.12$. Further increases in k lead to a decay in the growth rate, and for $k > 3.46$ stability prevails for small wavenumber disturbances. Also shown is the corresponding mode behaviour obtained directly from the dispersion relation in (3.21). The qualitative behaviour is excellent. Figure 15 is a comparison of the behaviour of the unstable mode obtained from the third-order temporal hyperbolic dispersion relation (5.10) with that predicted from the third-order parabolic dispersion relation (6.12) and the corresponding mode from (3.21). The parabolic approximation offers a substantially better qualitative approximation of the behaviour of the mode than the hyperbolic approximation, predicting a wavenumber with a maximum growth rate and a wavenumber above which disturbances are stable. Figure 16 shows the behaviour of $\mathrm{Re}(\lambda)$ and $\mathrm{Im}(\lambda)$ for the unstable mode predicted from (6.12) for $Q = 7.5$, $E = 20$ and $\gamma = 1.1$, a regime which is unstable to one-dimensional disturbances. As k increases from $k = 0$, the growth rate again increases monotonically with k before reaching a maximum at $k = 1.31$. Further increases in k again lead to a decay in the growth rate and for $k > 4.42$ stability prevails. Thus even though the detonation wave is unstable to one-dimensional disturbances, the maximum growth rate is attained

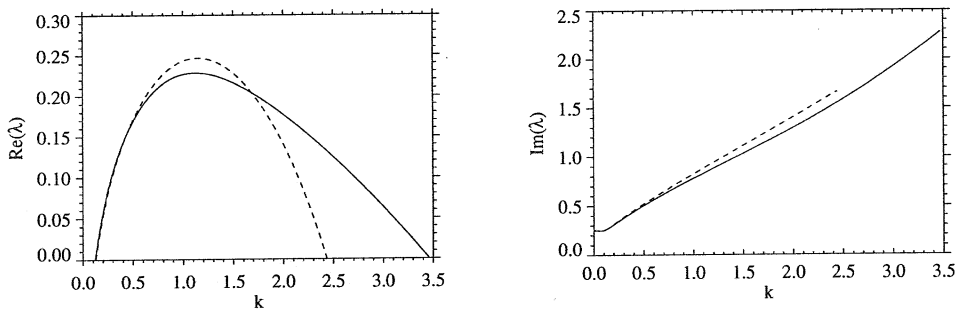

Figure 14. The variation of (a) $\mathrm{Re}(\lambda)$ and (b) $\mathrm{Im}(\lambda)$ from (6.12) with $Q = 10$, $E = 10$ and $\gamma = 1.1$ (solid lines). Also shown is the corresponding mode obtained from (3.21) (dashed lines).

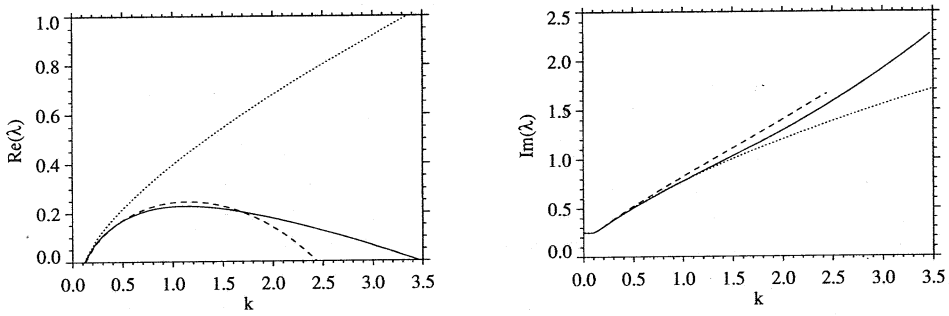

Figure 15. A comparison of the three modes obtained from the hyperbolic approximation (5.10) (dotted lines), the parabolic approximation (6.12) (solid lines) and from (3.21) (dashed lines) for $Q = 10$, $E = 10$ and $\gamma = 1.1$.

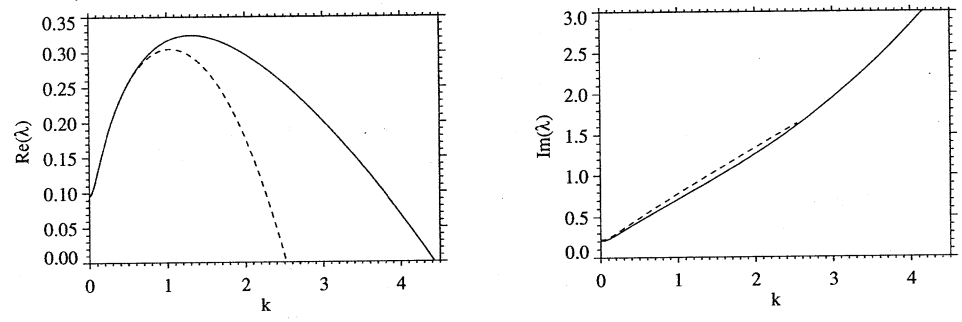

Figure 16. The variation of (a) $\mathrm{Re}(\lambda)$ and (b) $\mathrm{Im}(\lambda)$ from (6.12) with $Q = 7.5$, $E = 20$ and $\gamma = 1.1$ (solid lines). Also shown is the corresponding mode obtained from (3.21) (dashed lines).

away from $k = 0$, indicating the cellular instability should dominate the pulsating instability. For sufficiently large k the mode attenuates.

Thus the asymptotically derived, dispersive linear evolution equation (6.2), which is third-order in time and sixth-order in space, has all the correct physical features corresponding to the dynamics associated with exact linear dispersion

relations for cellular detonation stability. In particular, in appropriate parameter regimes, it predicts a two-dimensional neutral stability curve, a one-dimensional neutral stability curve, a maximum unstable growth rate for a finite value of the wavenumber, and finally a wavenumber above which all disturbances decay. In summary, lower-order evolution equations are shown not to contain sufficient information about the role of acoustic wave propagation or the effects of curvature of the front in the induction zone to accurately describe the dynamics of the onset of cellular instability. On the other hand, the generic features of the parabolic evolution equation (6.2) make it a favourable candidate for describing the initial dynamics of cellular detonation formation.

The work was supported by the U.S. Air Force Office of Scientific Research, Mathematics (F49620-96-1-0260). The author is grateful to Prof. D.S. Stewart and Prof. J.D. Buckmaster for their helpful insights, and to Prof. J.F. Clarke for valuable discussions of his unpublished three-dimensional, mean-flow generalisation of the nonlinear Clarke equation.

References

Abouseif, G. & Toong, T.Y. 1982 Theory of unstable one-dimensional detonations, *Combust. Flame* **45**, 64–94.

Blythe, P.A. & Crighton, D.G. 1989 Shock generated ignition: the induction zone. *Proc. R. Soc. Lond. A* **426**, 189–209.

Bourlioux, A., Majda, A.J. & Roytburd, V. 1991 Theoretical and numerical structure for unstable one-dimensional detonations, *SIAM J. Appl. Math.* **51**, 303–343.

Bourlioux, A. & Majda, A.J. 1992 Theoretical and numerical structure for unstable two-dimensional detonations. *Combust. Flame* **90**, 211–229.

Buckmaster, J.D. & Ludford, G.S.S. 1986 The effect of structure on the stability of detonations I. Role of the induction zone. In *Twenty-first Symposium (International) on Combustion,* The Combustion Institute. pp. 1669–1676.

Buckmaster, J.D. 1988 Pressure transients and the genesis of transverse shocks in unstable detonations. *Combust. Sci. Tech.* **61**, 1–20.

Buckmaster, J.D. & Neves, J. 1988 One-dimensional detonation stability: The spectrum for infinite activation energy. *Phys. Fluids* **31**, 3571–3576.

Buckmaster, J.D. 1989 A theory for triple point spacing in overdriven detonation waves. *Combust. Flame* **77**, 219–228.

Clarke, J.F. 1981 Propagation of gas-dynamic disturbances in an explosive atmosphere. *Progr. Astro. Aero.* **76**, 383–402.

Quirk, J.J. 1994 Godunov-type schemes applied to detonation flows. In *Combustion in high-speed flows* (eds. J. Buckmaster, T.L. Jackson & A. Kumar). Kluwer. pp. 575–596.

Short, M. 1996 An asymptotic derivation of the linear stability of the square wave detonation using the Newtonian limit. *Proc. Roy. Soc. A* **452**, 2203–2224.

Short, M. 1997 Multi-dimensional linear stability of a detonation wave at high-activation energy. *SIAM J. Appl. Math.* **57**, 307–326.

Short, M. & Stewart, D.S. 1997 Low-frequency two-dimensional linear instability of plane detonation. *J. Fluid Mech.* **340**, 249–295.

Stewart, D.S., Aslam, T.D. & Yao, J. 1996 On the evolution of cellular detonation. In *Twenty-sixth Symposium (International) on Combustion,* The Combustion Institute, Pittsburgh. pp. 2981-2989.

Williams, D.N., Bauwens, L. & Oran, E.S. 1996 Detailed structure and propagation of three-dimensional detonations. In *Twenty-sixth Symposium (International) on Combustion,* The Combustion Institute, Pittsburgh. pp. 2991-2998.

Yao, J. & Stewart, D.S. 1996 On the dynamics of multi-dimensional detonation waves. *J. Fluid Mech.* **309**, 225-275.

Zaidel, R.M. 1961 The stability of detonation waves in gaseous detonations. *Dokl. Akad. Nauk SSSR (Phys. Chem. Sect.)* **136**, 1142–1145.

Appendix A. Steady detonation parameters

For a given non-dimensional heat release Q, scaled with respect to the thermal energy in the fluid ahead of the detonation shock, the steady Chapman-Jouguet Mach number D_{CJ} is given by

$$D_{CJ} = \left[\left(1+\frac{(\gamma^2-1)}{\gamma}Q\right)+\sqrt{\left(1+\frac{(\gamma^2-1)}{\gamma}Q\right)^2-1}\right]^{\frac{1}{2}}. \tag{A 1}$$

The pressure jump across the detonation shock is given by

$$\nu = \frac{2\gamma D_{CJ}^2+1-\gamma}{\gamma+1}. \tag{A 2}$$

The post-shock temperature-scaled heat release β and activation energy θ are then related to their pre-shock temperature-scaled values Q and E by

$$\beta = \frac{(\gamma-1)}{\gamma}\frac{\mu}{\nu}Q, \quad \theta = \frac{\mu}{\nu}E. \tag{A 3}$$

The ratios σ_p and σ_ρ of the equilibrium zone pressure and density to their pre-shock values can be calculated from the Rankine-Hugoniot relations as

$$\sigma_p = \frac{1+\gamma D_{CJ}^2}{1+\gamma}, \quad \sigma_\rho = \frac{(\gamma+1)D_{CJ}^2}{1+\gamma D_{CJ}^2} \tag{A 4}$$

The constants μ_b and ν_b in §2 are finally evaluated as

$$\mu_b = \frac{\sigma_\rho}{\mu}, \quad \nu_b = \left(\frac{\mu}{\nu}\frac{\sigma_p}{\sigma_\rho}\right)^{\frac{1}{2}}. \tag{A 5}$$

Appendix B. Polynomial dispersion relation coefficents

$$\begin{aligned} C_1 \;=\; & (R_1+\gamma R_4)\left(\kappa_p-\frac{(\gamma-1)M_s^2\kappa_T}{(\gamma M_s^2-1)}\right)+R_2\left(\kappa_u+\frac{(\gamma-1)M_s\kappa_T}{(\gamma M_s^2-1)}\right) \\ & +R_3\left[\frac{(\gamma-1)(M_s^2-1)}{\beta(\gamma M_s^2-1)}\kappa_T\right]+R_5 \end{aligned} \tag{B 1}$$

$$C_2 = -R_5\kappa_T \tag{B 2}$$

$$
\begin{aligned}
C_3 \;=\; & \frac{(R_1+\gamma R_4)}{(M_s^2-1)}\left[-M_s\kappa_p+\kappa_u+\frac{(\gamma-1)M_s}{(\gamma M_s^2-1)}\left(2M_s^2\kappa_T+\kappa_p-M_s\kappa_u\right)\right] \\
& +\frac{R_2}{(M_s^2-1)}\left[-M_s\kappa_u+\kappa_p+(\gamma-1)\left(\frac{1}{(\gamma M_s^2-1)}\right.\right. \\
& \left.\left.\left[-(3M_s^2-1)\kappa_T-\kappa_p+M_s\kappa_u\right]\right)\right] \\
& +\frac{(\gamma-1)(M_s^2-1)}{\beta(\gamma M_s^2-1)}R_3\left[-\frac{2\kappa_T}{M_s}+\frac{\kappa_u}{(M_s^2-1)}-\frac{\kappa_p}{M_s(M_s^2-1)}\right] \\
& -(\gamma-1)\frac{\kappa_T}{M_s}R_4
\end{aligned}
\tag{B 3}
$$

$$
\begin{aligned}
C_4 \;=\; & \frac{\kappa_v}{(M_s^2-1)}\left[(R_1+\gamma R_4)M_s\left(1-(\gamma-1)\frac{M_s^2}{(\gamma M_s^2-1)}\right)\right. \\
& \left.-R_2\left(1-(\gamma-1)\frac{M_s^2}{(\gamma M_s^2-1)}\right)+(\gamma-1)\frac{M_s(M_s^2-1)}{\beta(\gamma M_s^2-1)}R_3\right]
\end{aligned}
\tag{B 4}
$$

$$
C_5 = R_5\left[-\left(-\frac{\kappa_T}{M_s}+\frac{\kappa_u}{2(M_s^2-1)}-\frac{\kappa_p}{2M_s(M_s^2-1)}\right)\right] \tag{B 5}
$$

$$
\begin{aligned}
C_6 \;=\; & \frac{(R_1+\gamma R_4)}{(M_s^2-1)^2}\left[\frac{(M_s^2+1)\kappa_p}{2}-M_s\kappa_u+(\gamma-1)\left(\frac{1}{2(\gamma M_s^2-1)}\right.\right. \\
& \left.\left.\left[-(3M_s^4-3M_s^2-4)\kappa_T-(4M_s^2+1)\kappa_p+(3M_s^2+2)M_s\kappa_u\right]\right)\right] \\
& +\frac{R_2}{(M_s^2-1)^2}\left[\frac{(M_s^2+1)\kappa_u}{2}-M_s\kappa_p+(\gamma-1)\left(\frac{1}{4M_s(\gamma M_s^2-1)}\right.\right. \\
& \left.\left.\left[2(5M_s^2-9)M_s^2\kappa_T+(11M_s^2-1)\kappa_p-(9M_s^2+1)M_s\kappa_u\right]\right)\right] \\
& +R_3\left[\frac{(\gamma-1)(M_s^2-1)}{\beta(\gamma M_s^2-1)}\left(\frac{3\kappa_T}{2M_s^2}-\frac{(3M_s^2-1)\kappa_u}{2M_s(M_s^2-1)^2}+\frac{(2M_s^2-1)\kappa_p}{M_s^2(M_s^2-1)^2}\right)\right] \\
& -\frac{(\gamma-1)}{M_s}R_4\left[-\frac{\kappa_T}{M_s}+\frac{\kappa_u}{2(M_s^2-1)}-\frac{\kappa_p}{2M_s(M_s^2-1)}\right]
\end{aligned}
\tag{B 6}
$$

$$
C_7 = R_5\left[-\frac{M_s\kappa_v}{2(M_s^2-1)}\right] \tag{B 7}
$$

$$
\begin{aligned}
C_8 \;=\; & \frac{(R_1+\gamma R_4)}{(M_s^2-1)}\left[-\frac{\kappa_p}{2}-\frac{M_s^2\kappa_v}{(M_s^2-1)}+(\gamma-1)\left(\frac{M_s^2}{2(\gamma M_s^2-1)}\right.\right. \\
& \left.\left.\left[-\kappa_T+\kappa_p+\frac{(3M_s^2+2)}{(M_s^2-1)}\kappa_v\right]\right)\right] \\
& +\frac{R_2}{(M_s^2-1)}\left[\frac{\kappa_p}{2M_s}+\frac{(3M_s^2-1)\kappa_v}{2M_s(M_s^2-1)}+(\gamma-1)\left(\frac{M_s}{2(\gamma M_s^2-1)}\right.\right. \\
& \left.\left.\left[\kappa_T-\kappa_p-\frac{(9M_s^2+1)\kappa_v}{2(M_s^2-1)}\right]\right)\right] \\
& -R_3\frac{(\gamma-1)}{\beta(\gamma M_s^2-1)}\left(\frac{\kappa_p}{2}+\frac{(3M_s^2-1)\kappa_v}{2(M_s^2-1)}\right) \\
& -(\gamma-1)R_4\left[\frac{\kappa_v}{2(M_s^2-1)}\right]
\end{aligned}
\tag{B 8}
$$

$$
C_9=-R_5\left[\frac{\kappa_T}{2M_s^2}+\frac{(2M_s^2-1)\kappa_p}{3M_s^2(M_s^2-1)^2}-\frac{(3M_s^2-1)\kappa_u}{6M_s(M_s^2-1)^2}\right] \tag{B 9}
$$

$$
\begin{aligned}
C_{10} \;=\; & \frac{(R_1+\gamma R_4)}{(M_s^2-1)^3}\left[-\frac{M_s(M_s^2+3)\kappa_p}{6}+\frac{(3M_s^2+1)\kappa_u}{6}\right. \\
& +(\gamma-1)\left(\frac{1}{18M_s(\gamma M_s^2-1)}\left[3(9-8M_s^2-9M_s^4+4M_s^6)\kappa_T\right.\right. \\
& \left.\left.\left.+2(4M_s^2+15M_s^4-8)\kappa_p-(-11+15M_s^2+18M_s^4)M_s\kappa_u\right]\right)\Big] \\
& +\frac{R_2}{(M_s^2-1)^3}\left[-\frac{M_s(M_s^2+3)\kappa_u}{6}+\frac{(3M_s^2+1)\kappa_p}{6}\right. \\
& +(\gamma-1)\left(\frac{1}{3M_s(\gamma M_s^2-1)}\left[-\frac{1}{4M_s}(14M_s^6-49M_s^4+24M_s^2+3)\kappa_T\right.\right. \\
& \left.\left.\left.-\frac{1}{6M_s}(49M_s^4-25M_s^2-2)\kappa_p+\frac{1}{12}(63M_s^4-14M_s^2-5)\kappa_u\right]\right)\Big] \\
& +R_3\frac{(\gamma-1)(M_s^2-1)}{\beta(\gamma M_s^2-1)}\left[-\frac{2\kappa_T}{3M_s^3}-\frac{(10M_s^4-9M_s^2+3)\kappa_p}{6M_s^3(M_s^2-1)^3}\right. \\
& \left.+\frac{(6M_s^4-3M_s^2+1)\kappa_u}{6M_s^2(M_s^2-1)^3}\right] \\
& -\frac{(\gamma-1)}{M_s}R_4\left[\frac{\kappa_T}{2M_s^2}+\frac{(2M_s^2-1)\kappa_p}{3M_s^2(M_s^2-1)^2}-\frac{(3M_s^2-1)\kappa_u}{6M_s(M_s^2-1)^2}\right]
\end{aligned}
\tag{B 10}
$$

$$
C_{11}=R_5\left[\frac{\kappa_p}{6(M_s^2-1)}+\frac{(3M_s^2-1)\kappa_v}{6(M_s^2-1)^2}\right] \tag{B 11}
$$

$$
\begin{aligned}
C_{12} \;=\; & \frac{(R_1+\gamma R_4)}{(M_s^2-1)^2}\left[\frac{M_s\kappa_p}{2}-\frac{\kappa_u}{6}+\frac{M_s(3M_s^2+1)\kappa_v}{6(M_s^2-1)}\right.\\
& +(\gamma-1)\left(\frac{M_s}{18(\gamma M_s^2-1)}\left[3(3M_s^2-1)\kappa_T\right.\right.\\
& \left.\left.-(12M_s^2+5)\kappa_p-\frac{(-11+15M_s^2+18M_s^4)}{(M_s^2-1)}\kappa_v\right]\right)\Bigg]\\
& +\frac{R_2}{(M_s^2-1)^2}\left[\frac{\kappa_u}{6M_s}-\frac{(4M_s^2-1)\kappa_p}{6M_s^2}-\frac{(6M_s^4-3M_s^2+1)\kappa_v}{6M_s^2(M_s^2-1)}\right.\\
& +(\gamma-1)\left(\frac{1}{12(\gamma M_s^2-1)}\left[-(7M_s^2-3)\kappa_T\right.\right.\\
& \left.\left.+\frac{1}{3}(35M_s^2-1)\kappa_p+\frac{1}{3(M_s^2-1)}(63M_s^4-14M_s^2-5)\kappa_v\right]\right)\Bigg]\\
& +R_3\frac{(\gamma-1)(M_s^2-1)}{\beta(\gamma M_s^2-1)}\left[\frac{(4M_s^2-1)\kappa_p}{6M_s(M_s^2-1)^2}-\frac{\kappa_u}{6(M_s^2-1)^2}\right.\\
& \left.+\frac{(6M_s^4-3M_s^2+1)\kappa_v}{6M_s(M_s^2-1)^3}\right]\\
& +\frac{(\gamma-1)}{M_s}R_4\left[\frac{\kappa_p}{6(M_s^2-1)}+\frac{(3M_s^2-1)\kappa_v}{6(M_s^2-1)^2}\right]
\end{aligned}
\tag{B 12}
$$

$$
C_{13}=\frac{k_v}{6(M_s^2-1)^2}\left[-M_s(R_1+\gamma R_4)+R_2-\frac{(\gamma-1)M_s(M_s^2-1)}{\beta(\gamma M_s^2-1)}R_3\right] \tag{B 13}
$$

$$
C_{14}=R_5\left[\frac{\kappa_T}{6M_s^3}+\frac{(10M_s^4-9M_s^2+3)\kappa_p}{24M_s^3(M_s^2-1)^3}-\frac{(6M_s^4-3M_s^2+1)\kappa_u}{24M_s^2(M_s^2-1)^3}\right] \tag{B 14}
$$

$$
\begin{aligned}
C_{15} \;=\; & \frac{(R_1+\gamma R_4)}{(M_s^2-1)^4}\left[\frac{1}{24}\left(M_s^4+6M_s^2+1\right)\kappa_p-\frac{M_s}{6}\left(M_s^2+1\right)\kappa_u\right. \\
& +(\gamma-1)\left(\frac{1}{72M_s(\gamma M_s^2-1)}\left[-\frac{1}{M_s}\left(15M_s^8-54M_s^6-25M_s^4\right.\right.\right. \\
& \left.+92M_s^2-44\right)\kappa_T-\frac{1}{2M_s}\left(120M_s^6+22M_s^4-129M_s^2+63\right)\kappa_p \\
& \left.\left.+\frac{1}{2}\left(60M_s^6+54M_s^4-63M_s^2+25\right)\kappa_u\right]\right)\Bigg] \\
& +\frac{R_2}{(M_s^2-1)^4}\left[-\frac{M_s}{6}\left(M_s^2+1\right)\kappa_p+\frac{1}{24}\left(M_s^4+6M_s^2+1\right)\kappa_u\right. \\
& +(\gamma-1)\left(\frac{1}{72M_s^2(\gamma M_s^2-1)}\left[\frac{1}{M_s}\left(27M_s^8-144M_s^6+145M_s^4\right.\right.\right. \\
& \left.-34M_s^2-10\right)\kappa_T+\frac{1}{4M_s}\left(436M_s^6-419M_s^4+108M_s^2+27\right)\kappa_p \\
& \left.\left.-\frac{1}{4}\left(228M_s^6-117M_s^4+28M_s^2+13\right)\kappa_u\right]\right)\Bigg] \\
& +\frac{(\gamma-1)(M_s^2-1)}{\beta(\gamma M_s^2-1)}R_3\left[\frac{5}{24M_s^4}\kappa_T+\frac{(5M_s^6-1-6M_s^4+4M_s^2)}{6M_s^4(M_s^2-1)^4}\kappa_p\right. \\
& \left.-\frac{(4M_s^2-1-5M_s^4+10M_s^6)}{24M_s^3(M_s^2-1)^4}\kappa_u\right] \\
& +\frac{(\gamma-1)}{M_s}R_4\left[\frac{\kappa_T}{6M_s^3}+\frac{(10M_s^4-9M_s^2+3)\kappa_p}{24M_s^3(M_s^2-1)^3}-\frac{(6M_s^4-3M_s^2+1)\kappa_u}{24M_s^2(M_s^2-1)^3}\right]
\end{aligned}
\tag{B 15}
$$

$$
C_{16}=-R_5\left[\frac{(4M_s^2-1)\kappa_p}{24M_s(M_s^2-1)^2}-\frac{k_u}{24(M_s^2-1)^2}+\frac{(6M_s^4-3M_s^2+1)\kappa_v}{24M_s(M_s^2-1)^3}\right] \tag{B 16}
$$

$$
\begin{aligned}
C_{17} \;=\; & \frac{(R_1+\gamma R_4)}{(M_s^2-1)^3}\left[\frac{M_s}{6}\kappa_u-\frac{1}{12}\left(3M_s^2+1\right)\kappa_p-\frac{M_s^2(M_s^2+1)}{6(M_s^2-1)}\kappa_v\right.\\
& +(\gamma-1)\left(\frac{1}{36(\gamma M_s^2-1)}\left[-\left(9M_s^4-5M_s^2+2\right)\kappa_T\right.\right.\\
& +\frac{1}{4}\left(60M_s^4+34M_s^2-19\right)\kappa_p-\frac{1}{4}\left(6M_s^2+19\right)M_s\kappa_u\\
& \left.\left.+\frac{1}{4(M_s^2-1)}\left(60M_s^6+54M_s^4-63M_s^2+25\right)\kappa_v\right]\right)\Bigg]\\
& +\frac{R_2}{(M_s^2-1)^3}\left[-\frac{1}{24M_s^2}\left(5M_s^2-1\right)\kappa_u+\frac{1}{24M_s^3}\left(10M_s^4-3M_s^2\right.\right.\\
& \left.+1\right)\kappa_p+\frac{1}{24M_s^3(M_s^2-1)}\left(10M_s^6-5M_s^4+4M_s^2-1\right)\kappa_v\\
& +(\gamma-1)\left(\frac{1}{12(\gamma M_s^2-1)}\left[\frac{1}{M_s}\left(4M_s^4-3M_s^2+1\right)\kappa_T\right.\right.\\
& -\frac{1}{24M_s}\left(208M_s^4-63M_s^2+5\right)\kappa_p+\frac{1}{24}\left(31M_s^2+19\right)\kappa_u\\
& \left.\left.-\frac{1}{24M_s(M_s^2-1)}\left(228M_s^6-117M_s^4+28M_s^2+13\right)\kappa_v\right]\right)\Bigg]\\
& +\frac{(\gamma-1)(M_s^2-1)}{\beta(\gamma M_s^2-1)}R_3\left[-\frac{1}{24M_s^2(M_s^2-1)^3}\left(10M_s^4-3M_s^2+1\right)\kappa_p\right.\\
& +\frac{1}{24M_s(M_s^2-1)^3}\left(5M_s^2-1\right)\kappa_u\\
& \left.-\frac{1}{24M_s^2(M_s^2-1)^4}\left(4M_s^2-1-5M_s^4+10M_s^6\right)\kappa_v\right]\\
& -\frac{(\gamma-1)R_4}{24M_s(M_s^2-1)^2}\left[\frac{1}{M_s}\left(4M_s^2-1\right)\kappa_p-\kappa_u+\frac{(6M_s^4-3M_s^2+1)\kappa_v}{M_s(M_s^2-1)}\right]
\end{aligned}
\tag{B 17}
$$

$$
C_{18}=\frac{M_s\kappa_v}{24(M_s^2-1)^2}R_5 \tag{B 18}
$$

$$
\begin{aligned}
C_{19} \;=\; & \frac{(R_1+\gamma R_4)}{(M_s^2-1)^2}\left[\frac{\kappa_p}{24}+\frac{M_s^2}{6(M_s^2-1)}\kappa_v\right.\\
& \left.+(\gamma-1)\left(\frac{M_s^2}{72(\gamma M_s^2-1)}\left[\kappa_T-\frac{(6M_s^2+19)}{2(M_s^2-1)}\kappa_v\right]\right)\right]\\
& +\frac{R_2}{(M_s^2-1)^2}\left[-\frac{1}{24M_s}\kappa_p-\frac{(5M_s^2-1)}{24M_s(M_s^2-1)}\kappa_v\right.\\
& \left.+(\gamma-1)\left(\frac{M_s}{72(\gamma M_s^2-1)}\left[-\kappa_T+\frac{(31M_s^2+19)}{4(M_s^2-1)}\kappa_v\right]\right)\right]\\
& +\frac{(\gamma-1)(M_s^2-1)}{\beta(\gamma M_s^2-1)}R_3\left[\frac{\kappa_p}{24(M_s^2-1)^2}+\frac{(5M_s^2-1)\kappa_v}{24(M_s^2-1)^3}\right]\\
& +\frac{(\gamma-1)\kappa_v R_4}{24(M_s^2-1)^2}
\end{aligned}
\tag{B 19}
$$

$$C_{20} = \frac{M_s\kappa_v(R_1+\gamma R_4)}{120(M_s^2-1)^3}\left(1+\frac{(\gamma-1)M_s^2}{3(\gamma M_s^2-1)}\right) - \frac{R_2\kappa_v}{120(M_s^2-1)^3}\left(1+\frac{(\gamma-1)M_s^2}{3(\gamma M_s^2-1)}\right)+\frac{(\gamma-1)M_sR_3\kappa_v}{120\beta(\gamma M_s^2-1)(M^2-1)^2} \quad \text{(B 20)}$$

List of Recent TAM Reports

No.	Authors	Title	Date
774	Mittal, R., and S. Balachandar	Effect of three-dimensionality on the lift and drag of circular and elliptic cylinders—*Physics of Fluids* **7**, 1841–1865 (1995)	Oct. 1994
775	Stewart, D. S., T. D. Aslam, and J. Yao	On the evolution of cellular detonation	Nov. 1994 *Revised* Jan. 1996
776	Aref, H.	On the equilibrium and stability of a row of point vortices—*Journal of Fluid Mechanics* **290**, 167–181 (1995)	Nov. 1994
777	Cherukuri, H. P., T. G. Shawki, and M. El-Raheb	An accurate finite-difference scheme for elastic wave propagation in a circular disk—*Journal of the Acoustical Society of America*, in press (1996)	Nov. 1994
778	Li, L., and N. R. Sottos	Improving hydrostatic performance of 1–3 piezocomposites—*Journal of Applied Physics* **77**, 4595–4603 (1995)	Dec. 1994
779	Phillips, J. W., D. L. de Camara, M. D. Lockwood, and W. C. C. Grebner	Strength of silicone breast implants—*Plastic and Reconstructive Surgery* **97**, 1215–1225 (1996)	Jan. 1995
780	Xin, Y.-B., K. J. Hsia, and D. A. Lange	Quantitative characterization of the fracture surface of silicon single crystals by confocal microscopy—*Journal of the American Ceramics Society* **78**, 3201–3208 (1995)	Jan. 1995
781	Yao, J., and D. S. Stewart	On the dynamics of multi-dimensional detonation—*Journal of Fluid Mechanics* **309**, 225–275 (1996)	Jan. 1995
782	Riahi, D. N., and T. L. Sayre	Effect of rotation on the structure of a convecting mushy layer—*Acta Mechanica* **118**, 109–120 (1996)	Feb. 1995
783	Batchelor, G. K., and TAM faculty and students	A conversation with Professor George K. Batchelor	Feb. 1995
784	Sayre, T. L., and D. N. Riahi	Effect of rotation on flow instabilities during solidification of a binary alloy—*International Journal of Engineering Science* **34**, 1631–1645 (1996)	Feb. 1995
785	Xin, Y.-B., and K. J. Hsia	A technique to generate straight surface cracks for studying the dislocation nucleation condition in brittle materials—*Acta Metallurgica et Materialia* **44**, 845–853 (1996)	Mar. 1995
786	Riahi, D. N.	Finite bandwidth, long wavelength convection with boundary imperfections: Near-resonant wavelength excitation—*International Journal of Mathematics and Mathematical Sciences*, in press (1996)	Mar. 1995
787	Turner, J. A., and R. L. Weaver	Average response of an infinite plate on a random foundation—*Journal of the Acoustical Society of America* **99**, 2167–2175 (1996)	Mar. 1995
788	Weaver, R. L., and D. Sornette	The range of spectral correlations in pseudointegrable systems: GOE statistics in a rectangular membrane with a point scatterer—*Physical Review E* **52**, 341 (1995)	Apr. 1995
789	Students in TAM 293–294	Thirty-second student symposium on engineering mechanics, J. W. Phillips, coordinator: Selected senior projects by K. F. Anderson, M. B. Bishop, B. C. Case, S. R. McFarlin, J. M. Nowakowski, D. W. Peterson, C. V. Robertson, and C. E. Tsoukatos	Apr. 1995
790	Figa, J., and C. J. Lawrence	Linear stability analysis of a gravity-driven Newtonian coating flow on a planar incline	May 1995
791	Figa, J., and C. J. Lawrence	Linear stability analysis of a gravity-driven viscosity-stratified Newtonian coating flow on a planar incline	May 1995
792	Cherukuri, H. P., and T. G. Shawki	On shear band nucleation and the finite propagation speed of thermal disturbances—*International Journal of Solids and Structures*, in press (1996)	May 1995
793	Harris, J. G.	Modeling scanned acoustic imaging of defects at solid interfaces—Chapter in *IMA Workshop on Inverse Problems in Wave Propagation*, eds. G. Chevant, G. Papanicolaou, P. Sacks and W. E. Symes, 237–258, Springer-Verlag, New York (1996)	May 1995

List of Recent TAM Reports (cont'd)

No.	*Authors*	*Title*	*Date*
794	Sottos, N. R., J. M. Ockers, and M. J. Swindeman	Thermoelastic properties of plain weave composites for multilayer circuit board applications	May 1995
795	Aref, H., and M. A. Stremler	On the motion of three point vortices in a periodic strip—*Journal of Fluid Mechanics* **314**, 1–25 (1996)	June 1995
796	Barenblatt, G. I., and N. Goldenfeld	Does fully-developed turbulence exist? Reynolds number independence versus asymptotic covariance—*Physics of Fluids* **7**, 3078–3082 (1995)	June 1995
797	Aslam, T. D., J. B. Bdzil, and D. S. Stewart	Level set methods applied to modeling detonation shock dynamics—*Journal of Computational Physics*, **126**, 390–409 (1996)	June 1995
798	Nimmagadda, P. B. R., and P. Sofronis	The effect of interface slip and diffusion on the creep strength of fiber and particulate composite materials—Proceedings of the ASME Applied Mechanics Division **213**, 125–143 (1995)	July 1995
799	Hsia, K. J., T.-L. Zhang, and D. F. Socie	Effect of crack surface morphology on the fracture behavior under mixed mode loading—*ASTM Special Technical Publication* 1296, in press (1996)	July 1995
800	Adrian, R. J.	Stochastic estimation of the structure of turbulent fields—*Eddy Structure Identification*, ed. J. P. Bonnet, Springer: Berlin 145–196 (1996)	Aug. 1995
801	Riahi, D. N.	Perturbation analysis and modeling for stratified turbulence	Aug. 1995
802	Thoroddsen, S. T.	Conditional sampling of dissipation in high Reynolds number turbulence—*Physics of Fluids* **8**, 1333–1335	Aug. 1995
803	Riahi, D. N.	On the structure of an unsteady convecting mushy layer—*Acta Mechanica*, in press (1996)	Aug. 1995
804	Meleshko, V. V.	Equilibrium of an elastic rectangle: The Mathieu–Inglis–Pickett solution revisited—*Journal of Elasticity* **40**, 207–238 (1995)	Aug. 1995
805	Jonnalagadda, K., G. E. Kline, and N. R. Sottos	Local displacements and load transfer in shape memory alloy composites	Aug. 1995
806	Nimmagadda, P. B. R., and P. Sofronis	On the calculation of the matrix–reinforcement interface diffusion coefficient in composite materials at high temperatures—*Acta Metallurgica et Materialia*, **44**, 2711–2716 (1996)	Aug. 1995
807	Carlson, D. E., and D. A. Tortorelli	On hyperelasticity with internal constraints—*Journal of Elasticity* **42**, 91–98 (1966)	Aug. 1995
808	Sayre, T. L., and D. N. Riahi	Oscillatory instabilities of the liquid and mushy layers during solidification of alloys under rotational constraint—*Acta Mechanica* **121** , 143–152 (1997)	Sept. 1995
809	Xin, Y.-B., and K. J. Hsia	Simulation of the brittle–ductile transition in silicon single crystals using dislocation mechanics	Oct. 1995
810	Ulysse, P., and R. E. Johnson	A plane-strain upper-bound analysis of unsymmetrical single-hole and multi-hole extrusion processes	Oct. 1995
811	Fried, E.	Continua described by a microstructural field—*Zeitschrift für angewandte Mathematik und Physik*, **47**, 168–175 (1996)	Nov. 1995
812	Mittal, R., and S. Balachandar	Autogeneration of three-dimensional vortical structures in the near wake of a circular cylinder	Nov. 1995
813	Segev, R., E. Fried, and G. de Botton	Force theory for multiphase bodies—*Journal of Geometry and Physics*, in press (1996)	Dec. 1995
814	Weaver, R. L.	The effect of an undamped finite-degree-of-freedom "fuzzy" substructure: Numerical solutions and theoretical discussion—*Journal of the Acoustical Society of America* **100**, 3159–3164 (1996)	Jan. 1996
815	Haber, R. B., C. S. Jog, and M. P. Bendsøe	A new approach to variable-topology shape design using a constraint on perimeter—*Structural Optimization* **11**, 1–12 (1996)	Feb. 1996
816	Xu, Z.-Q., and K. J. Hsia	A numerical solution of a surface crack under cyclic hydraulic pressure loading	Mar. 1996

List of Recent TAM Reports (cont'd)

No.	*Authors*	*Title*	*Date*
817	Adrian, R. J.	Bibliography of particle velocimetry using imaging methods: 1917–1995—*Produced and distributed in cooperation with TSI, Inc., St. Paul, Minn.*	Mar. 1996
818	Fried, E., and G. Grach	An order-parameter based theory as a regularization of a sharp-interface theory for solid–solid phase transitions—*Archive for Rational Mechanics and Analysis,* in press (1996)	Mar. 1996
819	Vonderwell, M. P., and D. N. Riahi	Resonant instability mode triads in the compressible boundary-layer flow over a swept wing—*Physics of Fluids*, in press (1996)	Mar. 1996
820	Short, M., and D. S. Stewart	Low-frequency two-dimensional linear instability of plane detonation—*Journal of Fluid Mechanics*, in press (1997)	Mar. 1996
821	Casagranda, A., and P. Sofronis	On the scaling laws for the consolidation of nanocrystalline powder compacts—Proceedings of the IUTAM Symposium on the Mechanics of Granular and Porous Materials (1996)	Apr. 1996
822	Xu, S., and D. S. Stewart	Deflagration-to-detonation transition in porous energetic materials: A comparative model study—*Journal of Fluid Mechanics*, in press (1997)	Apr. 1996
823	Weaver, R. L.	Mean and mean-square responses of a prototypical master/fuzzy structure—*Journal of the Acoustical Society of America*, in press (1996)	Apr. 1996
824	Fried, E.	Correspondence between a phase-field theory and a sharp-interface theory for crystal growth—*Continuum Mechanics and Thermodynamics*, in press (1997)	Apr. 1996
825	Students in TAM 293–294	Thirty-third student symposium on engineering mechanics, J. W. Phillips, coordinator: Selected senior projects by W. J. Fortino II, A. A. Mordock, and M. R. Sawicki	May 1995
826	Riahi, D. N.	Effects of roughness on nonlinear stationary vortices in rotating disk flows—*Mathematical and Computer Modeling,* in press (1996)	June 1996
827	Riahi, D. N.	Nonlinear instabilities of shear flows over rough walls	June 1996
828	Weaver, R. L.	Multiple scattering theory for a plate with sprung masses: Mean and mean-square responses	July 1996
829	Moser, R. D., M. M. Rogers, and D. W. Ewing	Self-similarity of time-evolving plane wakes	July 1996
830	Lufrano, J. M., and P. Sofronis	Enhanced hydrogen concentrations ahead of rounded notches and cracks—Competition between plastic strain and hydrostatic constraint	July 1996
831	Riahi, D. N.	Effects of surface corrugation on primary instability modes in wall-bounded shear flows	Aug. 1996
832	Bechel, V. T., and N. R. Sottos	Measuring debond length in the fiber pushout test—Proceedings of the ASME Mechanics and Materials Conference (1996)	Aug. 1996
833	Riahi, D. N.	Effect of centrifugal and Coriolis forces on chimney convection during alloy solidification—*Journal of Crystal Growth*, in press (1997)	Sept. 1996
834	Cermelli, P., and E. Fried	The influence of inertia on configurational forces in a deformable solid—*Proceedings of the Royal Society of London A*, in press (1996)	Oct. 1996
835	Riahi, D. N.	On the stability of shear flows with combined temporal and spatial imperfections	Oct. 1996
836	Carranza, F. L., B. Fang, and R. B. Haber	An adaptive space–time finite element model for oxidation-driven fracture	Nov. 1996
837	Carranza, F. L., B. Fang, and R. B. Haber	A moving cohesive interface model for fracture in creeping materials	Nov. 1996
838	Balachandar, S., R. Mittal, and F. M. Najjar	Properties of the mean wake recirculation region in two-dimensional bluff body wakes—*Journal of Fluid Mechanics*, in press (1997)	Dec. 1996

List of Recent TAM Reports (cont'd)

No.	Authors	Title	Date
839	Ti, B. W., W. D. O'Brien, Jr., and J. G. Harris	Measurements of coupled Rayleigh wave propagation in an elastic plate	Dec. 1996
840	Phillips, W. R. C.	On finite-amplitude rotational waves in viscous shear flows	Jan. 1997
841	Riahi, D. N.	Direct resonance analysis and modeling for a turbulent boundary layer over a corrugated surface	Jan. 1997
842	Liu, Z.-C., R. J. Adrian, C. D. Meinhart, and W. Lai	Structure of a turbulent boundary layer using a stereoscopic, large format video-PIV	Jan. 1997
843	Fang, B., F. L. Carranza, and R. B. Haber	An adaptive discontinuous Galerkin methods for viscoplastic analysis	Jan. 1997
844	Xu, S., T. D. Aslam, and D. S. Stewart	High-resolution numerical simulation of ideal and non-ideal compressible reacting flows with embedded internal boundaries	Jan. 1997
845	Zhou, J., C. D. Meinhart, S. Balachandar, and R. J. Adrian	Formation of coherent hairpin packets in wall turbulence	Feb. 1997
846	Lufrano, J. M., P. Sofronis, and H. K. Birnbaum	Elastoplastically accommodated hydride formation and embrittlement	Feb. 1997
847	Keane, R. D., N. Fujisawa, and R. J. Adrian	Unsteady non-penetrative thermal convection from non-uniform surfaces	Feb. 1997
848	Aref, H., and M. Brøns	On stagnation points and streamline topology in vortex flows	Mar. 1997
849	Asghar, S., T. Hayat, and J. G. Harris	Diffraction by a slit in an infinite porous barrier	Mar. 1997
850	Shawki, T. G., H. Aref, and J. W. Phillips	Mechanics on the Web—Proceedings of the International Conference on Engineering Education (Aug. 1997, Chicago)	Apr. 1997
851	Stewart, D. S., and J. Yao	The normal detonation shock velocity–curvature relationship for materials with non-ideal equation of state and multiple turning points	Apr. 1997
852	Fried, E., A. Q. Shen, and S. T. Thoroddsen	Traveling waves, standing waves, and cellular patterns in a steadily forced granular medium	Apr. 1997
853	Boyland, P. L., H. Aref, and M. A. Stremler	Topological fluid mechanics of stirring	Apr. 1997
854	Parker, S. J., and S. Balachandar	Viscous and inviscid instabilities of flow along a streamwise corner	May 1997
855	Soloff, S. M., R. J. Adrian, and Z.-C. Liu	Distortion compensation for generalized stereoscopic particle image velocimetry	May 1997
856	Zhou, Z., R. J. Adrian, S. Balachandar, and T. M. Kendall	Mechanisms for generating coherent packets of hairpin vortices in near-wall turbulence	June 1997
857	Neishtadt, A. I., D. L. Vainshtein, and A. A. Vasiliev	Chaotic advection in a cubic Stokes flow	June 1997
858	Weaver, R. L.	Ultrasonics in an aluminum foam	July 1997
859	Riahi, D. N.	High gravity convection in a mushy layer during alloy solidification	July 1997
860	Najjar, F. M., and S. Balachandar	Low-frequency unsteadiness in the wake of a normal flat plate	Aug. 1997
861	Short, M.	A parabolic linear evolution equation for cellular detonation instability	Aug. 1997